

THESIS

EXPERIMENTAL FATIGUE EVALUATION OF UNDERWATER STEEL PANELS
RETROFITTED WITH FIBER REINFORCED POLYMERS

Submitted by

Lauren Hudak

Department of Civil and Environmental Engineering

In partial fulfilment of the requirements

For the Degree of Master of Science

Colorado State University

Fort Collins, Colorado

Fall 2019

Master's Committee

Advisor: Hussam Mahmoud

Guillermo Riveros

Rebecca Atadero

Erin Arneson

Copyright by Lauren Hudak 2019

All Rights Reserved

ABSTRACT

EXPERIMENTAL FATIGUE EVALUATION OF UNDERWATER STEEL PANELS RETROFITTED WITH FIBER REINFORCED POLYMERS

Many steel structures are susceptible to fatigue loading and damage that can potentially threaten their integrity if not monitored and repaired. Steel hydraulic structures (SHS), in particular, experience fatigue loading during operation and are exposed to harsh environmental conditions that can further reduce fatigue life through mechanisms such as stress corrosion cracking and corrosion fatigue. Dewatering to complete inspections or repairs to SHS is time consuming and leads to economic losses, and current repair methods, such as rewelding, often cause new cracks to form after relatively few cycles, requiring repeated inspection and repair. The use of bonded carbon fiber reinforced polymer (CFRP) to repair fatigue cracks in metallic structures has been successfully demonstrated in other industries, and recent work has suggested that the method can also offers a more reliable repair method for SHS.

The very few studies regarding CFRP retrofits of SHS indicate that early bond failure often controls the degree of fatigue life extension provided by the repair. This study aims to extend previous experimental studies and further increase the fatigue life of repaired steel components by employing methods to improve CFRP bonding. Additionally, the use of basalt reinforced polymer (BFRP) as an alternative to CFRP is proposed. Limited examples of BFRP used in structural applications are available, but BFRP is attractive for SHS because it does not react galvanically with steel as CFRP does.

In this study, four large-scale center-cracked panels were tested under constant amplitude

fatigue loading. Of the four specimens, one was retrofitted with CFRP, and one was retrofitted with BFRP. To achieve an environment similar to that experienced by SHS, the two retrofitted specimens and one unretrofitted specimen were submerged in fresh water during testing. Remaining fatigue life was used as the primary metric for assessing the efficacy of the retrofit method. Results indicated that the use of both CFRP and BFRP are effective at extending fatigue life. The extent of fatigue life extension was still controlled by the quality of the FRP bond to steel; however, bond behavior was improved in comparison to previous underwater applications.

ACKNOWLEDGEMENTS

Thank you to my advisor, Dr. Mahmoud, for all his technical guidance, but most importantly, for keeping me motivated through the repeated challenges in the lab while also supporting my future goals.

A special thanks goes to Dr. Guillermo Riveros and Christine Lozano of the Engineering Research and Development Center at the U.S. Army Corps of Engineers for all their guidance, support, and visits to CSU. The financial support for the project through the U.S. Army Corps of Engineers is also greatly appreciated.

Matthew Szydowski of the machine shop at the Engineering Research Center was instrumental in the completion of this project. He not only built and maintained the test set-up, but was always willing to have brainstorming sessions, answer my many questions, and help keep me levelheaded through the challenges.

I also greatly appreciate all the generous help in the lab from Emad, Mazin, Kellan, and Mohamed, the help and support from my friends Lubna and Roman who were always willing to lend a hand, and the support of my boyfriend, Michael, who listened to me talk about the same things over and over and came along on many evening trips to the lab to take measurements.

TABLE OF CONTENTS

ABSTRACT.....	ii
ACKNOWLEDGEMENTS.....	iv
LIST OF TABLES.....	vii
LIST OF FIGURES.....	viii
Chapter 1: Introduction.....	1
1.1 Problem Statement.....	1
1.2 Objectives and Scope.....	5
1.3 Organization of Thesis.....	7
Chapter 2: Background and Literature Review.....	9
2.1 Introduction.....	9
2.2 Overview of CFRP Repairs of Center-Cracked Panels.....	9
2.2.1 Factors Contributing to CFRP Fatigue Repairs of Center-Cracked Panels.....	10
2.2.2 Methods for Improving FRP Bonding.....	13
2.3 Use of Basalt Fiber Reinforced Polymer.....	16
2.4 Underwater FRP Repair of Fatigue Cracks.....	18
2.4.1 Underwater Fatigue Crack Growth in Steel.....	18
2.4.2 Underwater Bonded FRP Durability.....	22
Chapter 3: Experimental Program.....	25
3.1 Introduction.....	25
3.2 Text Matrix and Specimen Details.....	25
3.3 Material Properties.....	28
3.4 Specimen Manufacture and Retrofit Application.....	29
3.5 Test Set-Up.....	32
3.6 Instrumentation.....	35
3.7 Test Procedure.....	37
Chapter 4: Experimental Results and Discussion.....	39
4.1 Introduction.....	39
4.2 Individual Specimen Results and Observations.....	39
4.2.1 Specimen 1.....	40
4.2.2 Specimen 2.....	47
4.2.3 Specimen 3.....	55
4.2.4 Specimen 4.....	64
4.3 Comparison of all Specimens.....	70
4.3.1 Comparison of Specimens 1 and 2.....	71
4.3.2 Comparison of Specimens 2 and 3.....	72
4.3.3 Comparison of Specimens 2 and 4.....	73
4.3.4 Comparison of Specimens 3 and 4.....	74

Chapter 5: Conclusion.....	77
5.1 Summary of Current Work.....	77
5.2 Conclusions	78
5.3 Recommendations for Future Work.....	79
References.....	81

LIST OF TABLES

Table 3-1. Test Matrix	27
Table 3-2. Material properties.....	29
Table 4-1. Specimen 1 Paris Law parameters for crack growth in mm and stress intensity factor in mm-MPa ^{1/2}	46
Table 4-2. Specimen 2 Paris Law parameters for crack growth in mm and stress intensity factor in mm-MPa ^{1/2}	53
Table 4-3. Paris Law parameters for air and marine environment provided by BS 7910 (2015). 54	

LIST OF FIGURES

Figure 1-1. crack near the pintle socket of a miter gate (Mahmoud & Riveros, 2013)	2
Figure 1-2. Cracks repaired by rewelding in miter gate girder and diaphragm flanges that experience compression loads during gate operation (HQUSACE, 2010).....	3
Figure 1-3. Welded window frame type repair implemented for gates at the Markland Locks and Dam.....	3
Figure 1-4. CFRP repair used underwater showing substantial debonding (Mahmoud et al., 2018)	5
Figure 2-1. Repair configurations used by Wu et al. (2012) (hatched areas represent CFRP, dimensions in mm).....	12
Figure 2-2. Crack growth results for various configurations as tested by Wu et al. (2012).....	12
Figure 2-3. Sketch of cross-section with adhesive spew fillet (Shield et al., 2004)	15
Figure 2-4. Clamp made from steel plates and pretensioned bolts to prevent CFRP debonding (Gangel, 2011)	15
Figure 2-5. S-N curves for glass, basalt, and carbon FRP developed by Dorigato and Pegoretti (2012).....	18
Figure 2-6. S-N curves for steel in air and fresh water corrosion fatigue (CF) (Morgantini et al., 2018)	21
Figure 2-7. Comparison of S-N curves for steel in fresh water and salt water (Morgantini et al., 2018)	21
Figure 2-8. Fatigue crack propagation of steel in solutions of varying pH (Misawa & Kobayashi, 2017)	22
Figure 3-1. Dimensions of center-cracked steel plates	26
Figure 3-2. Dimensions of retrofitted specimens.....	27
Figure 3-3. Cross-sectional view of FRP patches (not to scale).....	28
Figure 3-4. FRP patch retrofit application process	32
Figure 3-5. Schematic of self-reacting test frame looking south.....	34
Figure 3-6. Photo of test frame	35
Figure 3-7. Specimen 1 strain gauge layout.....	36
Figure 3-8. Specimen 2 strain gauge layout.....	36
Figure 3-9. Specimen 3 strain gauge layout.....	37
Figure 3-10. Specimen 4 strain gauge layout.....	37
Figure 4-1. North face of specimen 1 at early stage of test	41

Figure 4-2. Specimen 1 crack growth measurements	42
Figure 4-3. North face of Specimen 1 at test completion showing final length of east and west cracks and crack tip locations	43
Figure 4-4. Specimen 1 west crack surface indicating transition from stable to unstable crack growth	44
Figure 4-5. Specimen 1 west crack surface location near initial crack showing flat, smooth surface and indicating stable growth	44
Figure 4-6. Specimen 1 west crack surface location at large crack length showing slanted surface and indicating unstable growth	45
Figure 4-7. Plot of crack growth rate and stress intensity factor range for determination of Paris Law parameters for specimen 1	46
Figure 4-8. Specimen 1 strain in crack plane vs. half crack length	47
Figure 4-9. Specimen 2 before beginning test (prior to filling tank with water)	48
Figure 4-10. Specimen 2 underwater during test	48
Figure 4-11. Specimen 1 Crack Growth Measurements	49
Figure 4-12. South face of specimen 2 after test completion showing final crack lengths and crack tip locations	50
Figure 4-13. Specimen 2 east crack face showing transition from stable growth to unstable growth with increasing crack length	51
Figure 4-14. Specimen 2 east crack face location near initial crack showing flat surface and indicating stable growth	51
Figure 4-15. Specimen 2 east crack face location at large crack length showing slanted crack surface and indicating unstable growth	52
Figure 4-16. Plot of crack growth rate and stress intensity factor range for determination of Paris Law parameters for specimen 2	53
Figure 4-17. Specimen 2 north face strain in crack plane vs. half crack length	54
Figure 4-18. Specimen 2 south face strain in crack plane vs. half crack length	55
Figure 4-19. South face of specimen 3 before beginning test	56
Figure 4-20. Specimen 3 crack growth measurements	57
Figure 4-21. Debonding along edge of CFRP patch	58
Figure 4-22. North face of specimen 3 after fracture	59
Figure 4-23. South face of specimen 3 after fracture	59
Figure 4-24. CFRP patch on north side of specimen three with top half debonded after steel fracture	60
Figure 4-25. CFRP fracture of west patch on south face of specimen 3	61
Figure 4-26. CFRP fracture of east patch on south face of specimen 3	61

Figure 4-27. Specimen 3 strain in steel on crack plane	62
Figure 4-28. Specimen 3 west half strain in CFRP.....	63
Figure 4-29. North face of specimen 4 before beginning test.....	64
Figure 4-30. Specimen 4 crack growth measurements	65
Figure 4-31. North face of specimen 4 after fracture of west crack	66
Figure 4-32. South face of specimen 4 after fracture of west crack	66
Figure 4-33. Bond failure on upper half of southwest BFRP patch.....	67
Figure 4-34. Specimen 4 strain in steel.....	68
Figure 4-35. Specimen 4 strain in northwest BFRP patch.....	69
Figure 4-36. Specimen 4 strain in southwest BFRP patch	69
Figure 4-37. Comparison of crack growth for all specimens.....	70
Figure 4-38. Comparison of crack growth for specimens 1 and 2.....	71
Figure 4-39. Comparison of crack growth for specimens 2 and 3.....	73
Figure 4-40. Comparison of crack growth for specimens 2 and 4.....	74
Figure 4-41. Comparison of crack growth for specimens 3 and 4.....	75

CHAPTER 1

INTRODUCTION

1.1 Problem Statement

Many steel hydraulic structures (SHS) in the United States are approaching or have already surpassed their design service lives and are now susceptible to fatigue damage. Fluctuating load patterns are common in numerous civil engineering applications, but, for SHS, exposure to underwater environments and therefor accelerated corrosion can contribute to reduced fatigue life in comparison to other steel structures that are operating in less harsh conditions. Due to redundancy in most systems, repairing a single fatigue crack is at times not critical to safety and operation. However, large cracks or widespread cracking in multiple components can threaten the integrity of the structure or at the very least halt operation. In addition, the remaining fatigue life is difficult to quantify due to scatter in fatigue performance and the possible interaction of multiple flaws (Mahmoud, Chulawat, & Riveros, 2018; Mahmoud & Riveros, 2014).

Significant and extensive cracking has been repeatedly noted in SHS, especially in locations that are continuously submerged and not easily detectable without dewatering (USACE, 2010). Cracks are commonly noted at welded joints where residual stresses can cause tensile fatigue loading even if the location experiences compressive loading. Figure 1-1 and Figure 1-2 show examples of cracked miter gate components that are submerged during operation. Previous repair methods have imitated those used in the bridge industry, such as gouging and rewelding and adding welded cover plates (Mahmoud & Riveros, 2013). After repairing and resuming service,

these methods do not consistently offer long term solutions, as cracks tend to reinitiate after relatively few cycles due to newly introduced residual stresses.



Figure 1-1. crack near the pintle socket of a miter gate (Mahmoud & Riveros, 2013)

Fatigue cracks in welded joints in the miter gates at the Markland Locks and Dam on the Ohio River, for example, were first observed and repaired by gouging and rewelding in 1984 after 24 years in service. Four years after the first repairs, cracks at the previously repaired locations and new locations were noted. Triangular welded gusset plates were added to reduce stresses at the locations as shown in Figure 1-2. Six years later, cracking around the gusset plates was noticed, and the gusset plates were replaced with a window frame type repair as shown in Figure 1-3, successfully mitigated additional cracking (USACE, 2010). While existing repair methods can provide solutions to continue safe operation, frequent inspection and repair are still required afterwards. This is cumbersome and costly, as dewatering and inspection can require a structure to be temporarily taken out of service.



Figure 1-2. Cracks repaired by rewelding in miter gate girder and diaphragm flanges that experience compression loads during gate operation (HQUSACE, 2010)



Figure 1-3. Welded window frame type repair implemented for gates at the Markland Locks and Dam

Due to the challenges with existing repair methods, alternatives that are simple to implement and reliable are of interest. Recent work has proposed that fiber reinforced polymer (FRP) overlays offer a potential solution when used to repair cracks in SHS. Fiber reinforced polymers have long since been used for general strengthening and repair of structural components,

and, as summarized by Mahmoud and Riveros (2013), they have been shown to be effective when used to reduce the rate of fatigue crack propagation in metallic structures. However, the applicability of FRP repairs for fatigue in underwater environments has not been fully explored. Exposure to underwater environments accelerates crack growth and additionally can cause damage to and reduce the effectiveness of FRP repairs.

Recent large-scale underwater testing by Mahmoud, Riveros, Memari, Valsangkar, and Ahmadi (2018) demonstrated that carbon fiber reinforced polymers (CFRP) can be a viable option for underwater repairs, but their effectiveness was limited by poor adhesion to the steel substrate. Figure 1-4 shows a specimen that was repaired with CFRP and fatigue tested underwater exhibiting substantial CFRP debonding. Some of the debonding can be attributed to corrosion both from the underwater environment and from galvanic interaction between steel and the carbon fibers in contact with each other. When applied over a crack, FRP sheets reduce the stress intensity factor and therefore the crack propagation rate by reducing the nominal stress on the crack plane and providing a crack closure effect from the fibers that bridge the crack. Both factors rely on bonding between the cracked material and FRP to be effective; therefore, additional work is needed to maximize adhesion in an underwater environment to better increase the fatigue life of repaired cracks.

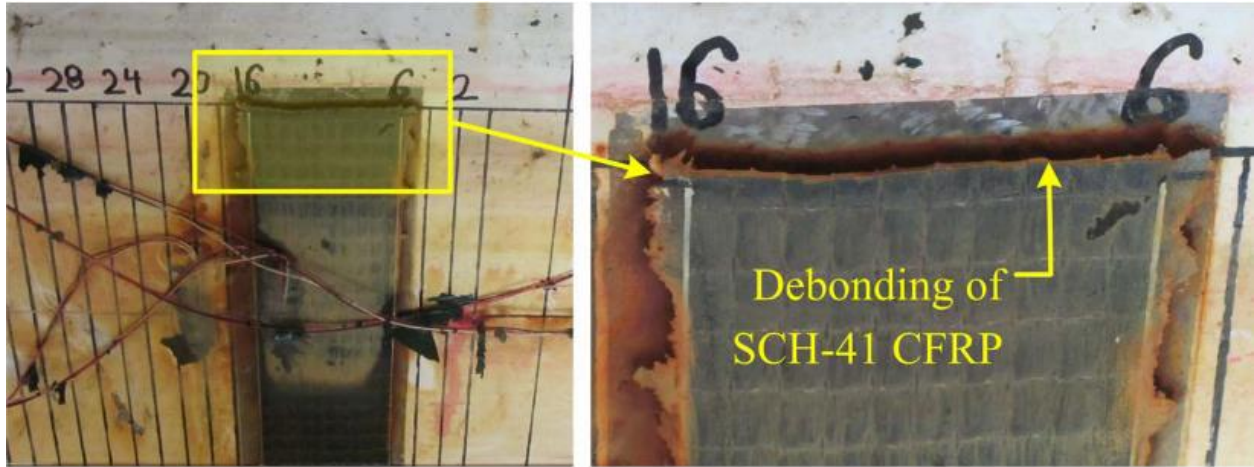


Figure 1-4. CFRP repair used underwater showing substantial debonding (Mahmoud et al., 2018)

For in-air applications, separation of the carbon and steel by means of an increased thickness adhesive layer or a layer of glass fibers has been used to reduce debonding due to galvanic corrosion. Use of alternative FRP materials other than CFRP, such as basalt fiber reinforce polymer (BFRP), that do not react with steel can also potentially reduce debonding if the material properties are suitable for the application. Aside from improving adhesion, previous studies on FRP repairs of fatigue cracks have shown improved fatigue life from varying the repair geometry by increasing the width of the FRP sheets to cover more of the crack plane or applying multiple FRP Layers. However, the methods common for enhancing repairs for in-air environments have not been extensively considered for their applicability in underwater environments.

1.2 Objectives and Scope

Before widespread use of FRP repairs for fatigue damage in SHS can be fully realized, a more complete understanding of the effects of an underwater environment is needed. Results from

the previously mentioned large-scale experimental work by Mahmoud et al. (2018) indicated that FRP repairs for improving fatigue life underwater are promising but in need of further assessment. Center-cracked steel panels were repaired with CFRP strips adhered ahead of the crack tips on both faces and fatigue tested to failure. When tested under water, the repair led to a fatigue life improvement of 1.16 times that of an unrepaired specimen underwater. The primary purpose of the work described herein is to build upon and improve the previously tested repair method. By increasing adhesion to steel, the applied FRP is more fully capable of reducing the stress intensity factor experienced by the crack. Varying the FRP repair geometry by increasing the width or using multiple layers can also increase the performance.

To accomplish the objective of improving and understanding FRP repairs for SHS, additional experiments needed to be conducted. Center-cracked steel panels similar to those previously tested were fabricated and then repaired. Debonding and corrosion were addressed by using thick adhesive layers, providing a separating layer of glass fiber for specimens repaired with CFRP, and introducing the use of BFRP as an alternative to CFRP. Specimens also include variations in repair width and number of FRP layers. Underwater fatigue tests with constant amplitude mode I-loading were conducted on each specimen. Results of the tests including fatigue life and crack growth rates can be used to assess the effectiveness of the repair approaches. The following tasks were used to realize the above objectives:

Task 1: Conduct a literature review

- Reassess factors most critical to FRP fatigue repairs
- Evaluate previous use of BFRP for steel structures
- Identify driving factors of underwater deterioration of steel and FRP

Task 2: Prepare test specimens and test set-up

- Design test matrix for investigating desired variables
- Apply the selected retrofit methods to the designated specimens
- Complete needed maintenance and modifications to the test set-up

Task 3: Execute experimental program

- Submerge specimens in water tank
- Apply fatigue loading to induce crack growth
- Collect readings of strain in steel and FRP
- Record crack length with corresponding number of cycles
- Observe bond behavior of FRP

Task 4: Interpret experimental results

- Evaluate and compare crack growth results across specimens
- Interpret recorded strain in FRP in conjunction with visually observed behavior
- Identify failure modes
- Assess effectiveness of CFRP and BFRP repairs

1.3 Organization of Thesis

This thesis is comprised of five chapters. The first addresses the need for an improved repair method for steel hydraulic structures with existing cracks and describes the purpose of this research towards meeting that need. Chapter 2 includes a literature review and background information regarding repair of structures with FRPs and their applicability to underwater environments. The experimental approach and test set-up are provided in Chapter 3. This includes details of the configuration of each specimen and the purpose of the selected configurations.

Results and discussion of the completed tests are presented in Chapter 4. Chapter 5 concludes the thesis by summarizing the findings of the work and addressing additional matters to be addressed in future work.

CHAPTER 2

BACKGROUND AND LITERATURE REVIEW

2.1 Introduction

Use of CFRP for repair of metal alloys has been well explored in recent years, although field use is still limited. Various experimental studies, several field application, and multiple numerical and analytical modeling approaches have been thoroughly reviewed by Mahmoud and Riveros (2013) for the purpose of assessing the applicability of CFRP use for SHS. Additionally, Riveros et al. (2019) covered the underlying fatigue and fracture topics related to fatigue crack repairs. Topics most critical to the success of CFRP fatigue crack repairs are reiterated in this chapter. Additionally, the factors introduced for underwater repairs and the proposed use of BFRP as an alternate to CFRP are considered.

2.2 Overview of CFRP Repairs of Center-Cracked Panels

Several examples of experimental programs using CFRP bonded to steel as fatigue crack repair method are available, and many express a purpose of repairing steel bridge components. Recently, Mahmoud and Riveros (2013) conducted a review of related experimental work, on metal alloys in general and steel structures specifically, as part of a feasibility study for CFRP repairs to hydraulic structures which can be referenced for a thorough assessment of previous experimental research. Here, the studies and topics most pertinent to the current experimental work are covered to highlight factors that affect the performance of CFRP when used to repair center-crack tension fatigue specimens.

2.2.1 Factors Contributing to CFRP Fatigue Repairs of Center-Cracked Panels

Two primary mechanisms from the addition of CFRP patches contribute to reducing fatigue crack growth (Colombi, 2004). First, increased stiffness from the patches reduces the nominal stress felt by the crack. Second, CFRP that bridges an existing crack limits the crack opening displacement. From the first mechanism, it follows that any increase in the stiffness of CFRP in the cracked cross-section can improve performance. The second mechanism only contributes if the CFRP is covering the crack. Increased stiffness also promotes reduction in crack opening displacement, but it is additionally imperative for the CFRP to be covering or as near as possible to the existing crack to utilize of the reduced crack opening effect. If the existing crack is not covered, the second mechanism is utilized only once the crack has propagated far enough to interact with the CFRP (i.e. under the CFRP patch). When extended, the fibers bridging the crack apply a compressive force that promotes crack closure. The effect is similar to that of compressive residual stresses that exist between stiffeners and reduce the crack rate in welded stiffened panels as demonstrated in several studies (Dexter, Mahmoud, & Pilarski, 2005; Dexter, Pilarski, & Mahmoud, 2003; H. N. Mahmoud & Dexter, 2005).

The method of increasing cross-section stiffness by using high modulus CFRP was demonstrated by Liu, Al-Mahaidi, and Zhao (2009) and Colombi and Fava (2015). High modulus CFRP is significantly more effective at improving fatigue life than an identical application of lower modulus CFRP. However, because higher modulus CFRP requires a greater stress to be transferred through the adhesive layer, adhesive can be more prone to debonding from steel during fatigue loading compared to when lower modulus CFRP is used if care is not taken to select an appropriate adhesive (Jones & Civjan, 2003).

Using thicker CFRP patches to increase the cross-section stiffness also improves fatigue

life in comparison to using a thinner layer as demonstrated by Liu, Al-Mahaidi, and Zhao (2009) and Colombi and Fava (2015). However, when a larger thickness is achieved by applying multiple layers of CFRP, the effectiveness of each subsequent layer is less than the previous layers due to reduced stress transfer to the outer layers (Liu, Xiao, Zhao, & Al-Mahaidi, 2009; Riveros, Mahmoud, & Lozano, 2018). Therefore, there may be a point when additional layers no longer provide significant benefit in terms of stress reduction at the crack tip.

Varying the width of applied CFRP patches can change the cross-section stiffness and can also, in conjunction with patch location along the crack plane, change the length of existing crack that is covered and experiences reduced crack opening displacement. The CFRP configurations used by Wu, Zhao, Al-mahaidi, Emdad, and Duan (2012) demonstrate the use of varying widths and locations along the crack plane well. Each CFRP configuration was applied to both sides of a steel plate with a crack initiator at the center, and specimens were fatigue tested with maximum stress of 150 MPa and stress ratio of 0.1 in the horizontal direction as shown in Figure 2-1. With maximum width and CFRP covering the initial crack, configuration (a) entirely arrested the crack. The other configurations still significantly increased fatigue life when compared to a specimen with no repair with an order from most to least improvement of (b), (e), (c), and (d) as shown in Figure 2-2. Results indicate that there is less improvement when the crack is not covered and, if not covered, when the patch is farthest away from the initial crack. Additional results were found by Jones and Civjan (2003) with similar style tests where fatigue life was improved by 170% when the initial crack was covered and 115% when it was not.

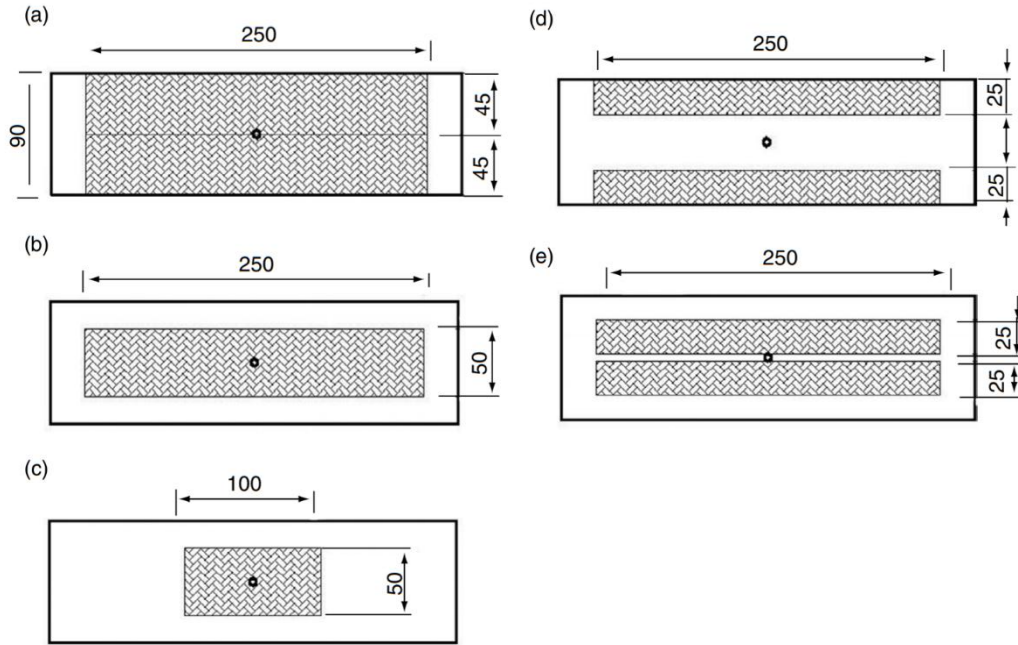


Figure 2-1. Repair configurations used by Wu et al. (2012) (hatched areas represent CFRP, dimensions in mm)

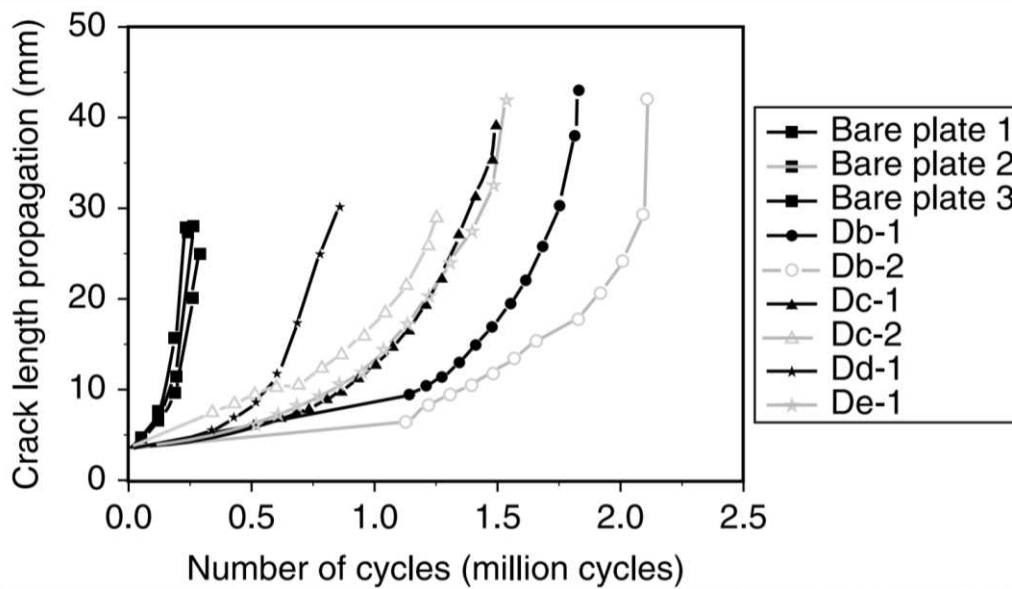


Figure 2-2. Crack growth results for various configurations as tested by Wu et al. (2012)

When comparing configurations (b) and (c) from Wu et al. (2012) it is clear that the length of an applied CFRP patch also contributes to repair effectiveness. However, performance is only

reduced when the CFRP length is less than the effective bond length. The effective bond length is the smallest length at which a maximum possible stress is reached in the CFRP (Nozaka, Shield, & Hajjar, 2005). Using a length greater than the effective length provides little to no additional benefit. Effective bond lengths for CFRP with steel substrate have been experimentally determined and estimated with empirical, analytical, and numerical models by both Lui, Zhao, Almahaidi, and Rizkalla (2007) and Nozaka et al. (2005).

Several studies have compared the use of single- and double-sided application of CFRP for fatigue repairs of cracked plates in tension (Jones & Civjan, 2003; Liu, Al-Mahaidi, et al., 2009; Mahmoud, Como, & Riveros, 2014; Zheng, Ye, & Lu, 2006). While single-sided repairs have been shown to be effective, double-sided repairs are considered to perform much better. A single-sided repair of a tensile member causes an eccentric load path leading to added bending stresses in the steel.

2.2.2 Methods for Improving FRP Bonding

Although use of bonded CFRP to repair fatigue cracks in steel has been shown to be effective, issues of debonding between adhesive and steel are common in previous testing and can significantly limit the repair effectiveness (Bocciarelli, Colombi, Fava, & Poggi, 2009; Colombi, Bassetti, & Nussbaumer, 2003b; Colombi & Fava, 2015; Jones & Civjan, 2003; Monfared, Soudki, & Walbridge, 2008; Riveros et al., 2019; Tavakkolizadeh & Saadatmanesh, 2003; Zheng et al., 2006). Debonding generally occurs where a stress concentration exists in the adhesive layer. Most predominantly, debonding begins either at the end of the CFRP patch or adjacent to the fatigue crack. The debonded portion then propagates beneath the CFRP, progressively reducing its effectiveness.

It may be possible to avoid any debonding at the CFRP patch ends as evidenced by fatigue

crack repair studies that did not observe any debonding prior to the final failure (Liu, Al-Mahaidi, et al., 2009; Mertz & Gillespie, 2002; Wu, Zhao, Al-Mahaidi, & Duan, 2013; Zhao & Zhang, 2007) and studies focused primarily on fatigue of CFRP bond to steel that report no debonding below threshold stress levels (Deng & Lee, 2007; Liu, Zhao, & Al-Mahaidi, 2005; Matta, Karbhari, & Vitaliani, 2005). The composite and adhesive properties selected must be appropriate for the required loading, and the loading must be relatively low. Liu et al. (2005), for example, found that bonds in double strap joints between steel and CFRP did not experience fatigue failure if the maximum fatigue stress was less than approximately 40% of the joint's ultimate strength.

Debonding adjacent to the fatigue crack likely cannot be prevented due to the very high strains near the crack tip, but reduced debonding at the crack may be attainable. Colombi et al. (2003b) reports that delamination around the crack occurs in an elliptical shape with a width that spans between the plastic zones at either end of a crack and a height that can vary depending on the system properties. Analytical models, such as that used by Lozano and Riveros (2019), can also be used to determine the local debonding near the crack. Lozano and Riveros (2019) used results from Mahmoud et al. (2018) for validation and found good agreement.

Bond between CFRP and steel can be improved by increasing the adhesive layer thickness because a larger shear deformation can be achieved before debonding occurs (Colombi et al., 2003b). Using an adhesive with high ductility similarly allows for more deformation before debonding (Nozaka et al., 2005). However, increasing the adhesive deformation can reduce the repair effectiveness because stress is transferred from the steel to the CFRP less efficiently. In locations where a patch covers the crack, adhesive deformation allows for a larger crack opening displacement (Colombi et al., 2003b). Despite reduced effectiveness due to thicker adhesive, preventing sizable debonded regions is more critical.

If material properties of the system cannot be modified to provide better bonding, several other techniques can be used to prevent debonding at patch ends. The use of a spew fillet around the edges of CFRP patches, as shown in Figure 2-3, is known to reduce the stress concentration at the end of the adhesive as suggested by Bocciarelli et al. (2009), Deng and Lee (2007), and Shield, Nozaka, and Hajjar (2004). Mechanical clamps, such as the example shown in Figure 2-4, can also be used to apply pressure at the end of CFRP patches to prevent debonding (Gangel, 2011; Vatandoost, 2010).

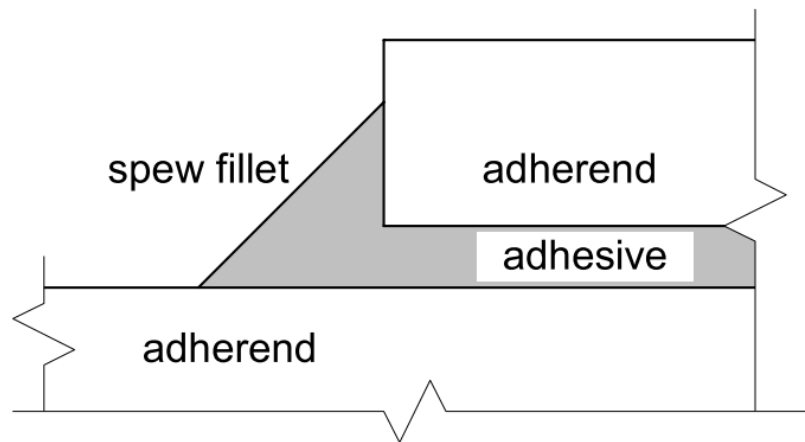


Figure 2-3. Sketch of cross-section with adhesive spew fillet (Shield et al., 2004)

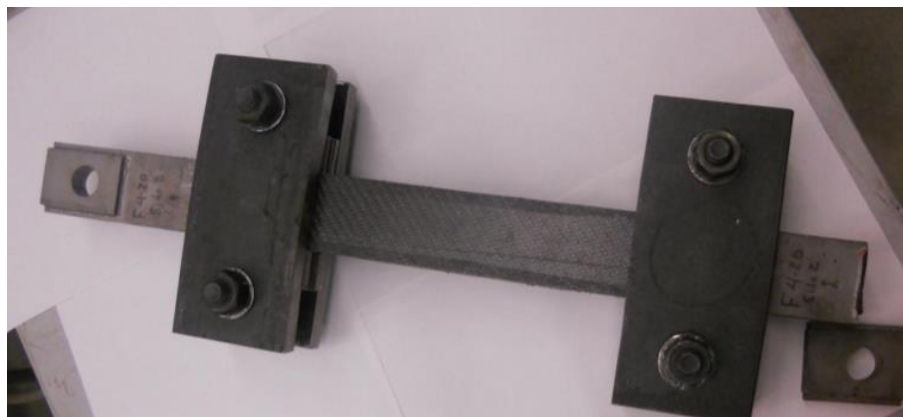


Figure 2-4. Clamp made from steel plates and pretensioned bolts to prevent CFRP debonding (Gangel, 2011)

An additional consideration for the bond between CFRP and steel is galvanic corrosion. When two dissimilar metals are in direct contact, a galvanic cell is formed, and the anode, which is steel in the case of steel and CFRP contact, corrodes (Tavakkolizadeh & Saadatmanesh, 2001). Corrosion forming between the CFRP and steel deteriorates the bond. To prevent galvanic action, the carbon and steel must be insulated from each other. Use of a thick layer of adhesive has been shown to be effective at reducing galvanic action (Tavakkolizadeh & Saadatmanesh, 2001). It is also common to use a layer of glass fiber fabric between steel and CFRP as insulation (Hollaway & Cadei, 2002; Liu, Al-Mahaidi, et al., 2009; Mertz & Gillespie, 2002; Zhao & Zhang, 2007).

2.3 Use of Basalt Fiber Reinforced Polymer

Use of BFRP in civil engineering applications is new and limited to only a few studies. A basalt and steel wire hybrid composite was used by Wu et al. (2012) to repair steel beams in fatigue, and BFRP was used by Jayasuriya, Bastani, Kenno, Bolisetti, and Das (2018) to restore the strength of steel beams with corrosion damage, but no other instances of BFRP used with steel structural components are known.

A key benefit of BFRP for applications to steel is that it does not cause galvanic corrosion. Basalt is not a conductor (Jayasuriya et al., 2018), so there is no concern of dissimilar metals coming in contact as is previously discussed with regard to carbon. Use of basalt may improve bonding in comparison by eliminating galvanic corrosion completely. Additionally, BFRP installation can be simplified because an extra step to insulate the FRP from the steel substrate is not necessary.

Mechanical properties of basalt fiber can vary widely, but basalt fibers have significantly lower tensile strength and modulus than carbon fibers and higher tensile strength and modulus than

glass fibers (Wu et al., 2012; Wu, Wang, Iwashita, Sasaki, & Hamaguchi, 2010). Since strength is generally controlled by the bond rather than the fibers for the proposed type of fatigue crack repairs, the reduced strength of BFRP compared to CFRP is not of highest concern. FRP stiffness, however, contributes significantly to repair effectiveness, and the lower modulus of BFRP would tend to reduce the crack closure effect.

It may be possible to account for the lower modulus of BFRP by using a larger thickness of BFRP when comparing its use to CFRP to obtain equivalent stiffnesses as was done by Wu et al. (2012). A variety of FRP types were used to repair notched steel beams tested in fatigue with thicknesses adjusted for each type to maintain the same stiffness of the repair across specimens. Comparable results for fatigue life improvement were found for the composites tested despite their variations in tensile modulus.

Due to previous use in other industries, fatigue life of BFRP has been studied. BFRP does not perform as well in fatigue as CFRP. Dorigato & Pegoretti (2012) developed S-N curves for carbon, basalt, and glass fiber laminates in tensile fatigue as shown in Figure 2-5. The slope of the S-N curve for BFRP is dramatically steeper than that for CFRP, indicating a reduced fatigue life in comparison to CFRP. Fatigue limits for CFRP and BFRP determined by Wu et al. (2010) indicated that BFRP has infinite life under constant amplitude fatigue when the stress is less than 55% of its tensile strength, whereas the same is true for CFRP when the stress is less than 84% of its tensile strength. Due to the lower fatigue resistance of BFRP, more fatigue life consideration of the composite may be needed when BFRP is used as an alternative to CFRP in fatigue repairs.

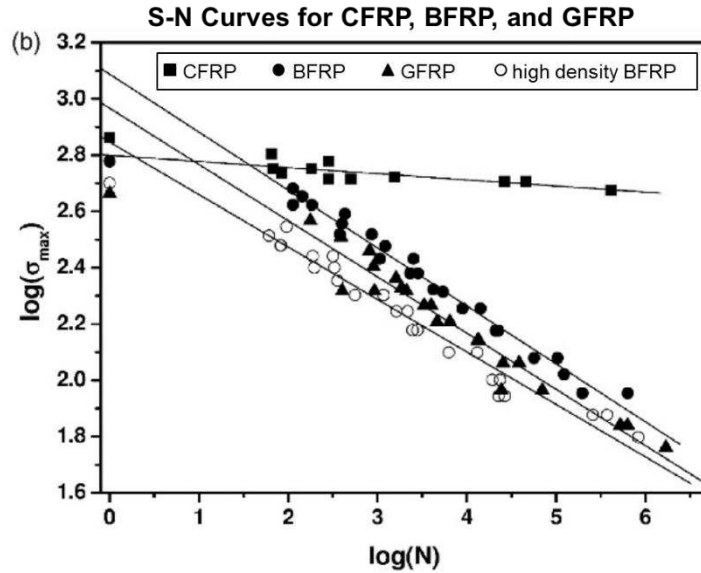


Figure 2-5. S-N curves for glass, basalt, and carbon FRP developed by Dorigato and Pegoretti (2012)

2.4 Underwater FRP Repair of Fatigue Cracks

It is well understood that the fatigue life of unprotected steel is reduced in an underwater environment, and the deleterious effect is known as corrosion fatigue. In addition to increased crack growth in steel due to the underwater environment, FRP repair methods may also be less effective when exposed to water. Although these effects are recognized, they are difficult to assess due to time dependence. In comparison to underwater structural repairs that can often be in place for many years, the time spans of existing experimental studies are short. It is possible that degradation may continue to increase with longer exposure time, however; information is limited because use of composites in civil engineering and especially in underwater environments is relatively new.

2.4.1 Underwater Fatigue Crack Growth in Steel

In comparison to fatigue in air, corrosion fatigue is more complex and requires the consideration of more variables such as load frequency and chemical properties of the water.

Although the exact contributions to corrosion fatigue remain unclear due to difficulty in differentiating between all mechanisms during experimentation, hydrogen embrittlement and anodic dissolution are commonly attributed as the main driving factors (Gangloff, 2009; Kang, Lee, & Kim, 2011; Salivar, Creighton, & Hoepfner, 1981). Hydrogen embrittlement increases crack growth rate by making the material around the crack more brittle. Hydrogen in water absorbs into crack surfaces and interferes with grain boundary cohesion. Anodic dissolution occurs as the newly exposed material from crack growth reacts with the water and is dissolved (Gangloff, 2009).

In air, loading frequency has little effect on fatigue crack growth rate in steels. However, in underwater environments, frequency becomes an important factor due to the time dependence of the chemical reactions that contribute to increased growth rates. A testing regime using lower frequency allows more time for reaction and therefore results in a more pronounced increase in crack growth underwater compared to in air. An experimental study conducted by Salivar et al. (1981) considered crack propagation in steel in air, distilled water, and saltwater environments with varying frequencies. Wedge opening load type specimens with 1-inch thicknesses were tested in air and in a chamber containing either distilled water or 3.5% NaCl solution. A frequency of 10 Hz in air was used as a baseline for comparison with other scenarios. For both distilled water and salt water, frequencies of 10 Hz, 1 Hz, and 0.1 Hz were tested. Resulting crack growth rates showed no significant difference between the three environments for the highest frequency of 10 Hz. For the lower frequencies, the underwater environments caused significantly higher crack growth rates with crack growth rate increasing with decreasing frequency. However, there was no significant difference between results for the distilled water and saltwater environments. Hydrogen embrittlement was attributed to the increased crack rates underwater as a result of the fractography analysis of the crack surfaces that was conducted and showed intergranular fracture was present

when the growth rate was increased in underwater environments.

Similarly, varying the stress range can indirectly introduce a time variable that affects fatigue life underwater. If maintaining all other variables, reducing the stress range lowers the crack growth rate and therefore increases the time required for a crack to grow to a given length. If underwater, the increased time needed for crack growth allows the environmental factors a longer time to react, resulting in more pronounced degradation. This can result in a larger difference between fatigue life in air and water with lower stress ranges compared to higher stress ranges. Plots of stress range versus number of cycles for air, fresh water, and saltwater environments were developed and compared by Morgantini, Okorokov, Gorash, Mackenzie, and Van Rijswick (2018). Round rod specimens were axially fatigue tested with varying stress ranges and stress ratios in the three environments. Comparing the resulting S-N curves for fresh water and air, as shown in Figure 2-6, indicates that the environmental factors are much more present with low stress ranges. At higher stress ranges, at which the tests took less than 10^6 cycles, the results in water showed little difference from those in air. However, at the lowest stress ranges tested, which approached 10^7 cycles, the fatigue life was reduced by a factor of 2.1 when in water. The authors attribute this to the larger amount of time in water when the stress range is low. It is also noted that the fatigue limit for the underwater environment was not reached in the stress ranges that were tested, which implies that the life reduction could be even greater with lower stress range. Comparing the resulting S-N curves in fresh water and salt water as shown in Figure 2-7 shows that salt water reduces fatigue life more so than fresh water, but the difference is very small compared to that between fresh water and air

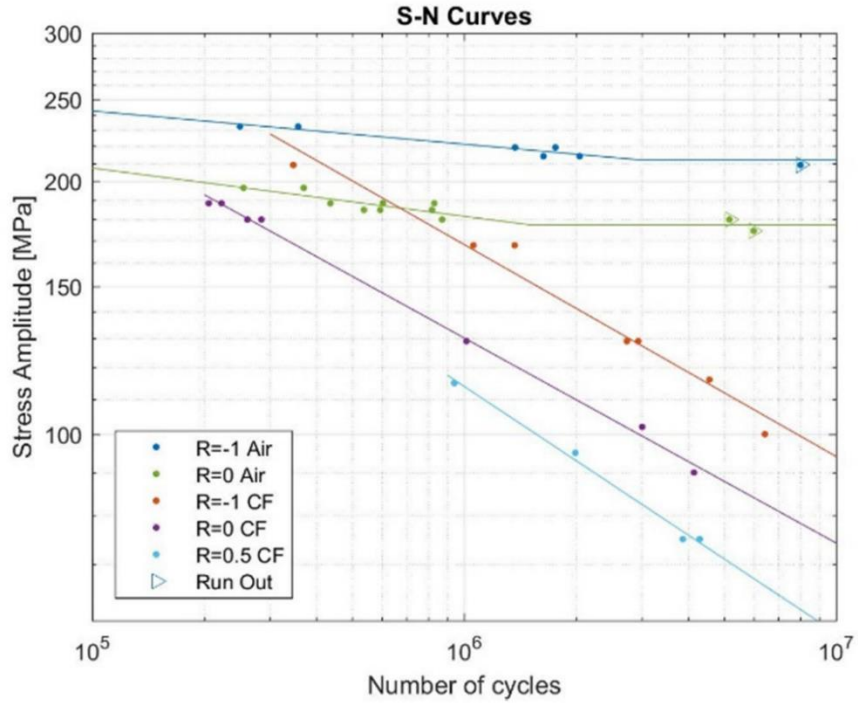


Figure 2-6. S-N curves for steel in air and fresh water corrosion fatigue (CF) (Morgantini et al., 2018)

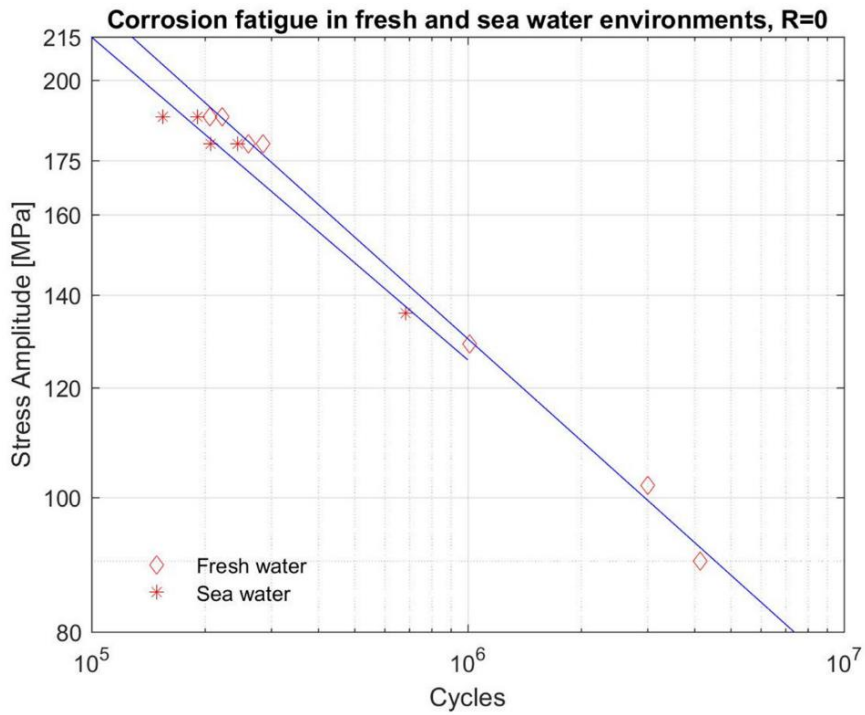


Figure 2-7. Comparison of S-N curves for steel in fresh water and salt water (Morgantini et al., 2018)

As one of the driving factors of corrosion fatigue is hydrogen embrittlement, which is caused by a reaction between steel and hydrogen, it is logical that the pH of the environment may affect fatigue life. Differences in fatigue life between steel in solutions of various acidities were explored by Misawa and Kobayashi (1976). Round rod specimens with 15 mm diameter and 2.5 mm machined notches were tested in a rotating-bending fatigue machine. A corrosion cell around the specimens contained water with pH of 0.5, 5.3, or 11.2. Crack length and number of cycles were recorded throughout each of the tests. The solution closest to neutral, with a pH of 5.3, resulted in the highest fatigue life. Both the acidic and basic solutions reduced the life; however, it was reduced significantly more with the acidic solution, as depicted in Figure 2-8. This suggests a complex relationship between the pH of water and fatigue life of steel.

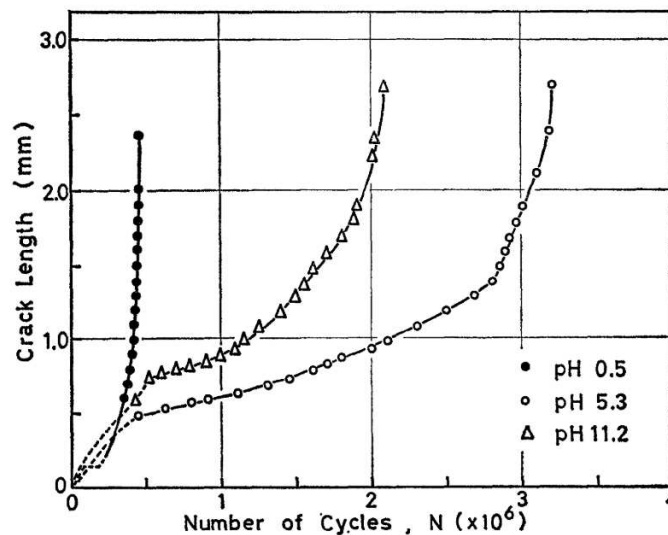


Figure 2-8. Fatigue crack propagation of steel in solutions of varying pH (Misawa & Kobayashi, 2017)

2.4.2 Underwater Bonded FRP Durability

As with in-air repairs, underwater repairs with FRP have been explored more so for concrete than steel applications. Several examples of applying FRP to deteriorated concrete in tidal zones have been completed (Al Azzawi, Hopkins, Mullins, & Sen, 2018; Long et al., 2012).

Mahmoud and Riveros (2013) provided a small number of examples of CFRP used for repair of ship structures. However, no examples of FRP used underwater for fatigue repair in steel other than those by Mahmoud et al. (2018) and Riveros et al. (2018) are known. Although limited, previous work has shown that tensile strength, elastic modulus, fatigue life, and bond of FRP can be reduced when underwater.

Changes in tensile strength and elastic modulus of various FRP including CFRP and BFRP after exposure to aqueous solutions were studied by Liu, He, and Xiong (2017). Coupons were subjected to wet-dry cycles where they were submerged for 15 days and then in air for 15 days. Tensile tests to obtain ultimate strength and tensile modulus were conducted after between 1 and 12 wet-dry cycles were completed. Sulfate, chloride, alkaline, and acidic solutions were used. The CFRP samples were minimally affected by all of the solutions with maximum reductions after 12 cycles of 10% and 5% for tensile strength and modulus, respectively. However, BFRP was more significantly degraded after 12 cycles with tensile strength reductions between 13% and 34% depending on solution type and tensile modulus reductions of approximately 15%.

In air, CFRP is well known for its high fatigue strength. CFRP coupons exposed to moisture were tested in bending fatigue and compared to dry specimens by Meng, Le, Grove, and Jahir Rizvi (2016). Samples were submerged in fresh water or sea water for three months prior to testing, and moisture was maintained during testing by wrapping them with saturated sponges. Tests used constant amplitude four-point bending with a stress ratio of 0.1 and various maximum stresses. Although resulting fatigue lives were scattered, saturated specimens clearly showed reduced life in comparison to dry specimens. Dry specimens tended to have infinite life, which was taken as no sign of failure after 3×10^6 cycles, if the maximum stress was less than 80% of ultimate strength. For saturated specimens, the life was generally only infinite if the maximum stress was less than

65% of ultimate strength.

The adhesives used for FRP can also be susceptible to damage from exposure to water. Water can diffuse into adhesives and chemically react (Hollaway & Cadei, 2002). It is possible for the adhesive to plasticize or breakdown and crack. Adhesive deterioration due to moisture exposure is known to be time dependent. However, no example of environmental testing with extended durations that would be applicable for civil engineering structures with long services lives is known, and accelerated testing methods do not represent the environments experienced in service well (Hollaway & Cadei, 2002).

CHAPTER 3

EXPERIMENTAL PROGRAM

3.1 Introduction

The experimental program consisted of testing four center-cracked steel panels, two of which were retrofitted with FRP, subjected to constant amplitude mode I fatigue loading. Both BFRP and CFRP were used to evaluate BFRP as an alternative to CFRP. Specimens were submerged in fresh water to simulate the service environment experienced by SHS. The specimen design, test frame, and procedure are similar to those previously used by Mahmoud et al. (2018).

3.2 Text Matrix and Specimen Details

The center-cracked steel plates tested were identical to those used by Mahmoud et al. (2018) with dimensions of 1 m by 1 m, a thickness of 9.5 mm (3/8 in), and centered 102 mm (4 in) precut crack as shown in Figure 3-1. Additionally, because only crack propagation, not initiation, was of interest, tack welds were placed at the ends of the pre-cut crack to promote the initial step of crack propagation from the precut crack. Dimensions were selected based on analysis completed and described by Mahmoud et al. (2018). One unretrofitted specimen (specimen 2) was tested in fresh water for comparison to the repaired specimens, while another unretrofitted specimen (specimen 1) was tested in air to determine the reduction in fatigue life in steel caused by the underwater environment.

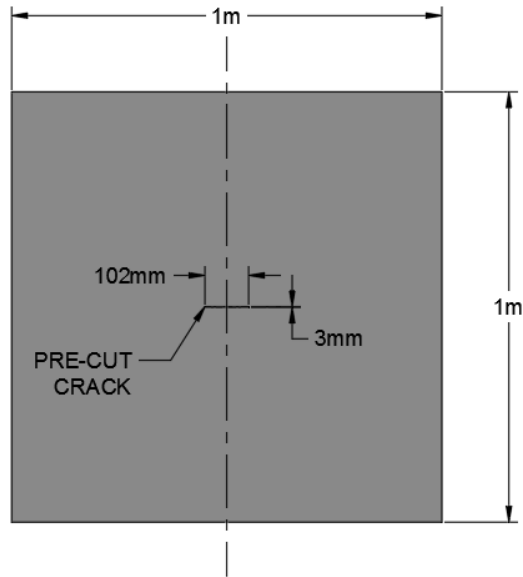


Figure 3-1. Dimensions of center-cracked steel plates

Two specimens were retrofitted with FRP patches on both faces. The retrofitted specimens were tested in fresh water to simulate the environment experienced by steel hydraulic structures since both the steel and FRP system can be deteriorated by moisture. It should be noted that treated fresh water was used as a baseline condition and river water that hydraulic structures are exposed to may be more complex and introduce more factors contributing to deterioration. An FRP patch width of 178 mm (7 in) was selected based on the manufactured width of the basalt fiber fabric that was used. A patch length of 381 mm (15 in) was used to be consistent with previous experiments conducted by Mahmoud et al. (2018). Both repaired specimens used two layers of FRP on each face. CFRP and BFRP were used for specimen 3 and specimen 4, respectively. The retrofit method and test environment for each specimen are summarized in Table 3-1. Figure 3-2 shows dimension of the retrofitted specimens.

Table 3-1. Test Matrix

Specimen	FRP Type	FRP Layers	Environment
1	None	0	Air
2	None	0	Fresh Water
3	Carbon	2	Fresh Water
4	Basalt	2	Fresh Water

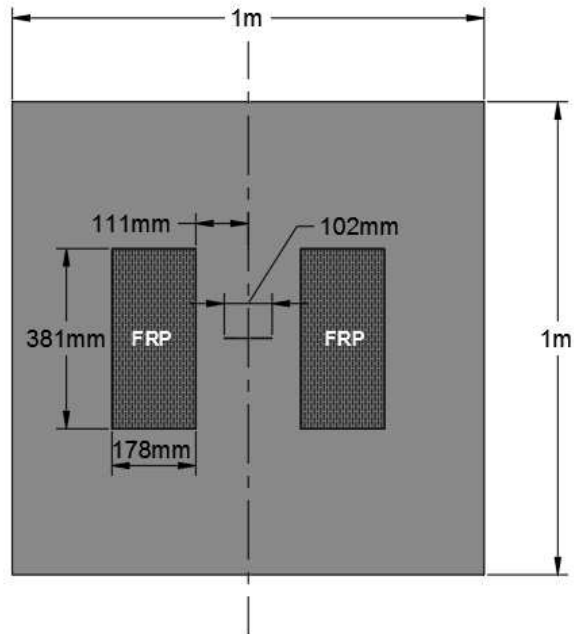


Figure 3-2. Dimensions of retrofitted specimens

An adhesive epoxy was used between the steel and FRP patch and between subsequent layers of FRP to improve bonding. A spew fillet was also formed from the adhesive around the perimeter of the FRP patch to reduce stress concentrations and prevent debonding at the patch ends. For the specimen repaired with CFRP, an additional layer of glass fiber fabric was installed between the steel and CFRP to provide an insulating barrier and prevent galvanic corrosion. Cross-sectional views of the FRP patch locations are illustrated in Figure 3-3.

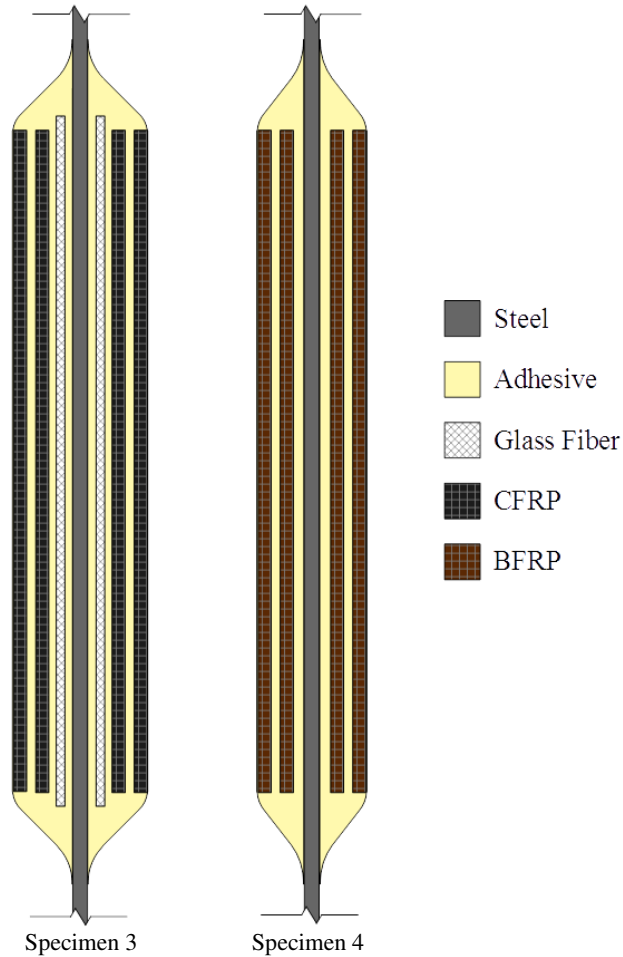


Figure 3-3. Cross-sectional view of FRP patches (not to scale)

3.3 Material Properties

Both types of FRP were made from unidirectional fiber fabrics that were saturated with epoxy to form composites. The carbon fabric used was Tyfo SCH-41, manufactured by Fyfe Co. The type and manufacturer of the basalt fibers are unknown. Tyfo S epoxy made by Fyfe Co. was used as the saturant epoxy for both fiber types. Tyfo TC epoxy made by Fyfe Co. was used as the adhesive. The mechanical properties of materials are provided in Table 3-2. Since the basalt fiber properties are unknown, ranges are listed in Table 3-2 as found in the literature (Dorigato &

Pegoretti, 2012; Liu, He, & Xiong, 2017; Wu, Wang, Wu, Liu, & Ren, 2012; Wu, Wang, Iwashita, Sasaki, & Hamaguchi, 2010). The plates used were structural rolled steel with 9.5 mm (3/8 in) thickness. A bi-directional glass fiber fabric was used for the insulation for the CFRP repaired specimen.

Table 3-2. Material properties

Material	Tensile Strength (MPa)	Tensile Modulus (GPa)
Steel	250	200
Carbon Fiber (Tyfo SCH-41)	4000	230
Basalt Fiber	1200-2200	65-90
Saturant Epoxy (Tyfo S)	72.4	3.18
Adhesive Epoxy (Tyfo TC)	22.7	1.2

Average thickness of the CFRP measured from coupons was approximately 2 mm. For the BFRP, average measured thickness from coupons was 3 mm. The CFRP and BFRP were not intended to have equivalent stiffness; although, the larger thickness of the BFRP can partially account for its reduced tensile modulus in comparison to the CFRP. Although adhesive application was not perfectly even, the average thickness of an adhesive layer was approximately 3 mm.

3.4 Specimen Manufacture and Retrofit Application

Each specimen was cut to size from 9.5 mm (3/8 in) rolled steel plates and then holes for connection to the testing frame were made with a magnetic drill. The existing crack was first cut with a 102 mm (4 in) diameter and 3 mm (1/8 in) thick angle grinder disk and then cut to square with a reciprocating saw. Tack welds, approximately 6 mm (1/4 in) in diameter, were added at the ends of the cracks to promote crack initiation.

For the retrofitted specimens, outlines of the FRP patch locations were marked, and an angle grinder was used to roughen the surface within the patch locations. The roughened surfaces were then thoroughly cleaned with acetone to remove particles from grinding, and the patch locations were re-marked. The required carbon, glass, and basalt fiber fabrics were cut to size and wiped with a cloth dampened with acetone to remove any dust. Glass fibers were cut approximately 13 mm (1/2 in) larger in both dimensions than the carbon fibers to ensure an adequate insulating layer should there be any slight misalignment during application.

A wet layup process was used to apply the FRP patches. Proper adhesion and fiber alignment were critical during the application process because they are important for the performance of the retrofit. However, the installation process was not intended to be highly precise because it is ultimately intended to be feasible for applications in the field rather than a controlled laboratory environment.

The adhesive (Tyfo-TC) and saturant (Tyfo-S) used are both two-component epoxies, and they were mixed according to manufacturer instructions. Each component was measured by weight, and an electric mixer was used to mix for the specified amount of time. The time was noted after mixing each batch of epoxy, and new batches were made as needed based on the manufacturer specified pot life.

FRP patches were applied one at a time. Adhesive was spread on the roughened steel surface in a uniform layer using a spatula. A layer of fibers was then placed on top of the adhesive and gently pressed into the adhesive and smoothed to remove any air bubbles and align fibers. Additional alternating layers of adhesive and fibers were applied as needed for each specimen. Before being placed, carbon fibers and basalt fibers were saturated with Tyfo-S. Fibers were fully submerged in the saturant and then removed and gently stripped of excess by hand. Placement was

such that the unidirectional fibers were aligned perpendicular to the crack plane. The glass fiber fabric layers were not saturated.

After all the layers were applied, spew fillets around the patches were formed by hand from additional adhesive to create a smooth transition between the patch and the steel. Any spilled or excess epoxy on the specimen was then removed. The epoxies were allowed to harden before being handled, and the manufacturer specified cure time was provided. The FRP application process is illustrated in Figure 3-4.

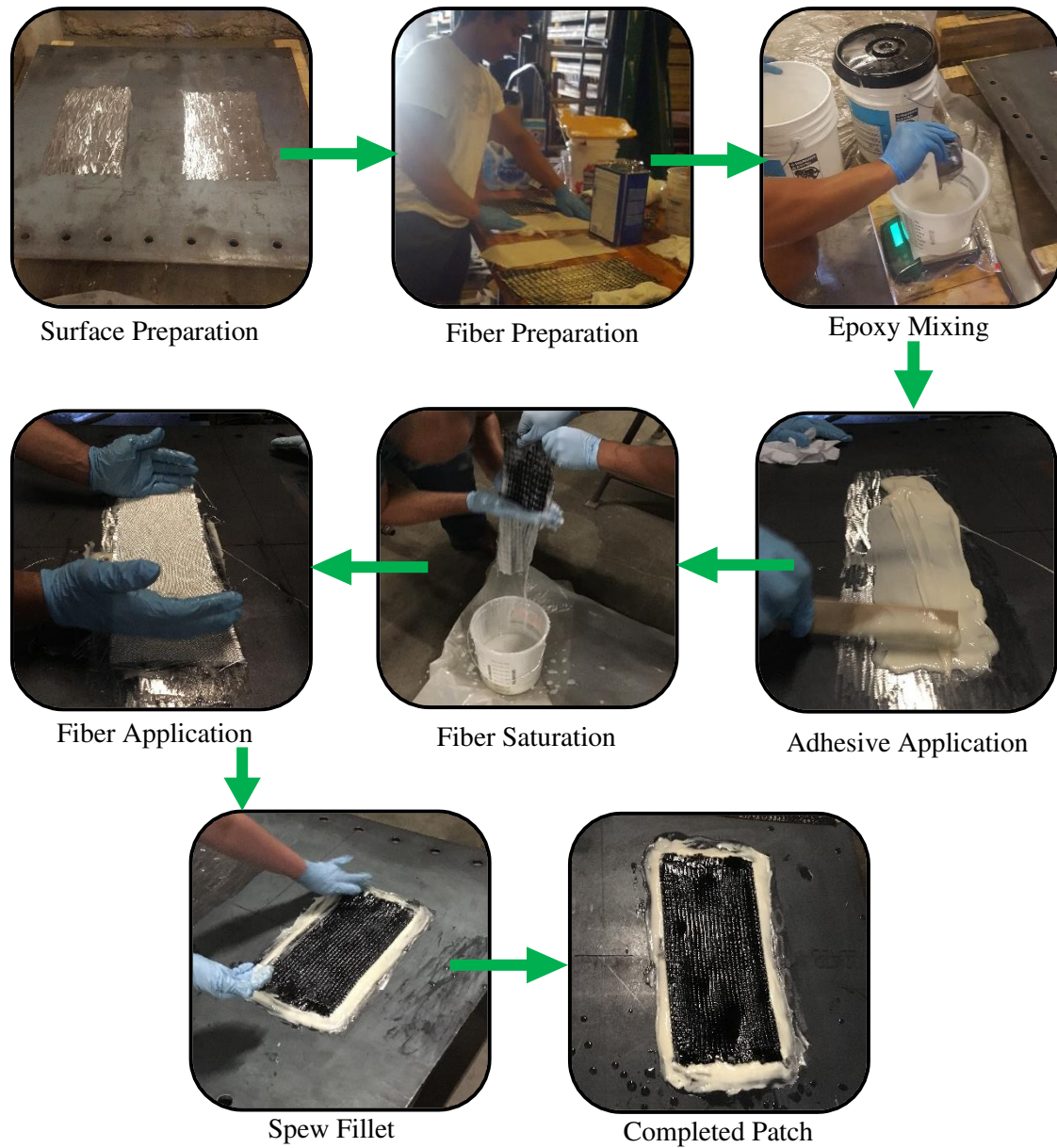


Figure 3-4. FRP patch retrofit application process

3.5 Test Set-Up

A self-reacting steel frame was designed to support the specimen and MTS hydraulic actuator and resist the cyclic load applied to the specimen. Conceptually, the test frame was identical to that used by Mahmoud et al. (2018), but beam and column sizes were increased to

extend the frame's fatigue life. Once installed, specimens were positioned such that the faces of the steel plates were oriented to the north and south and cracks would propagate to the east and west. Specimens were attached to the lower beam using a double angle connection. Another double angle connection at the top of the specimens attached a stiffened built-up I-beam used to distribute load from the actuator. The actuator was secured to the test frame's upper beam with threaded rods that spanned from the actuator through to the top flange of the beam. Strain gauges on the rods were used to monitor pretensioning of the rods. All bolts in the test frame were pretensioned using direct tension indicating washers.

A tank was built surrounding the specimens for use when an underwater test environment was needed. The steel tank floor rested on the lower test frame beam. Acrylic sheets were used as tank walls so that the specimens could be easily observed from outside the tank. Pumps were installed so that the tank could be easily filled and drained when needed. A schematic of the test frame and water tank as viewed looking south is provided in Figure 3-5. A photo of the test system viewed looking south is shown in Figure 3-6.

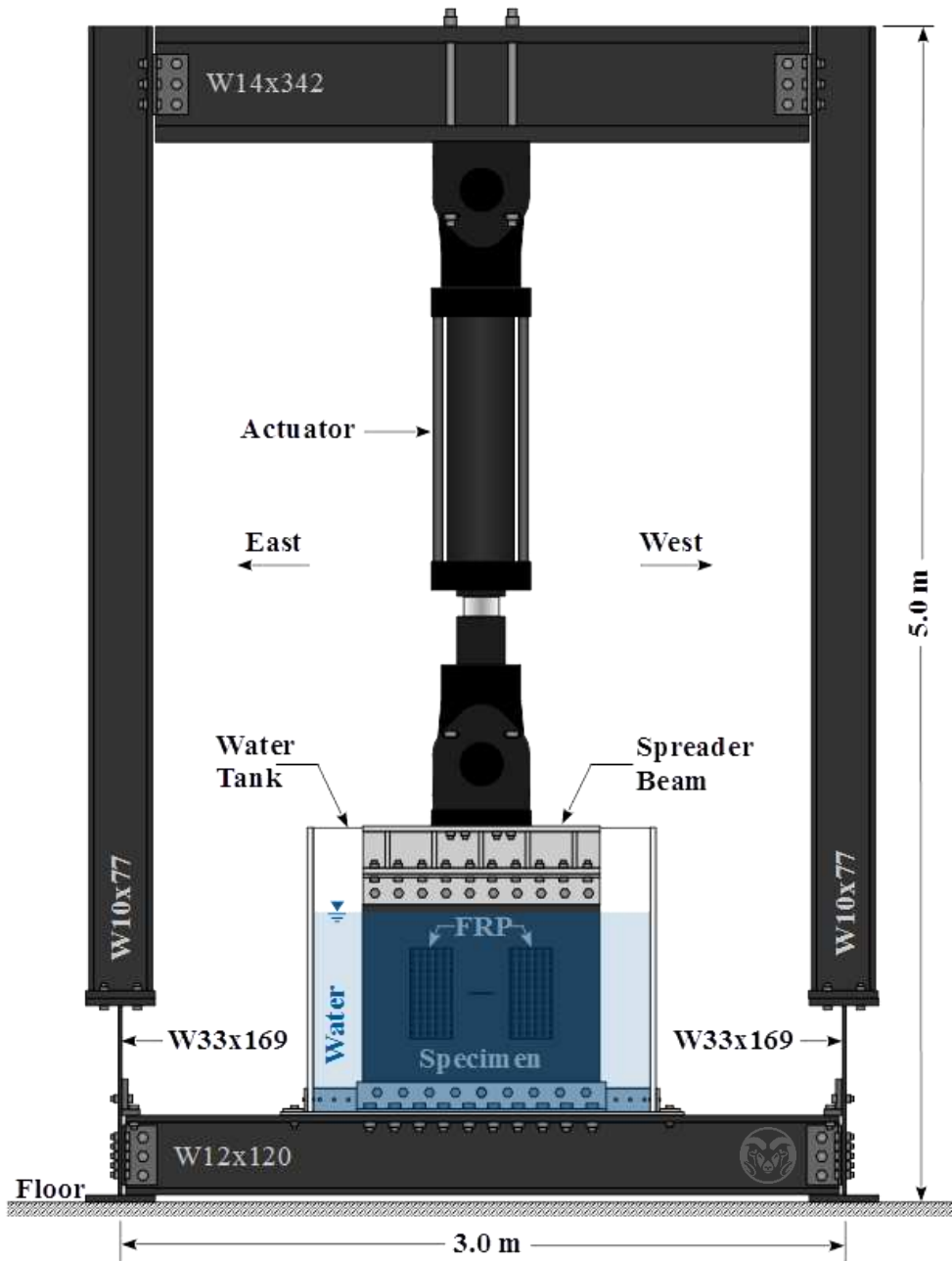


Figure 3-5. Schematic of self-reacting test frame looking south



Figure 3-6. Photo of test frame

3.6 Instrumentation

Strain gauges were installed on each specimen as shown in Figure 3-7 through Figure 3-10. Specimen 1 included strain gauges located above the crack plane to verify the applied nominal stress. All specimens had multiple strain gauges installed along the crack plane. Readings from these gauges were expected to increase with crack growth and grow rapidly as the crack

approached a gauge. For the retrofitted specimens, additional strain gauges were used to monitor FRP debonding, if any, by placing them along the height of the patches. A drop in a reading from a gauge on the FRP indicated that the bond directly beneath it was no longer intact. Strain gauges applied to specimens 2 through 4 were covered in silicone sealant to protect them from the water. A National Instruments PXI data acquisition system was used for recording strain readings.

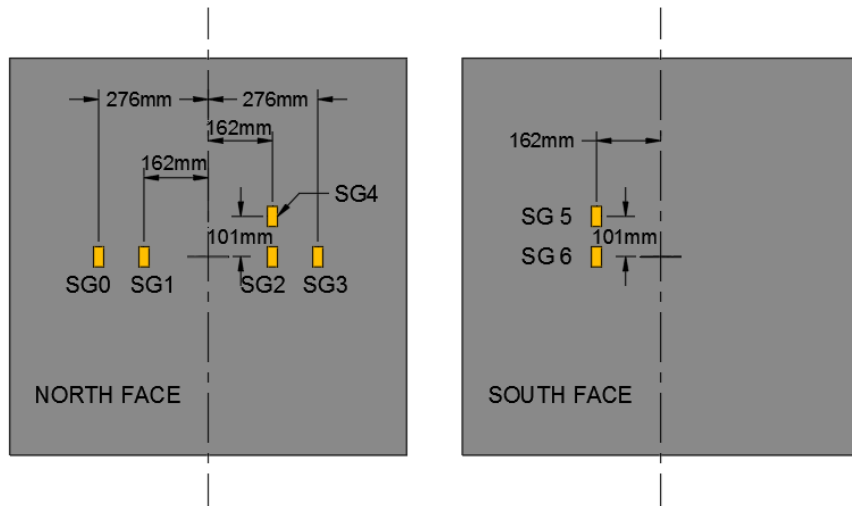


Figure 3-7. Specimen 1 strain gauge layout

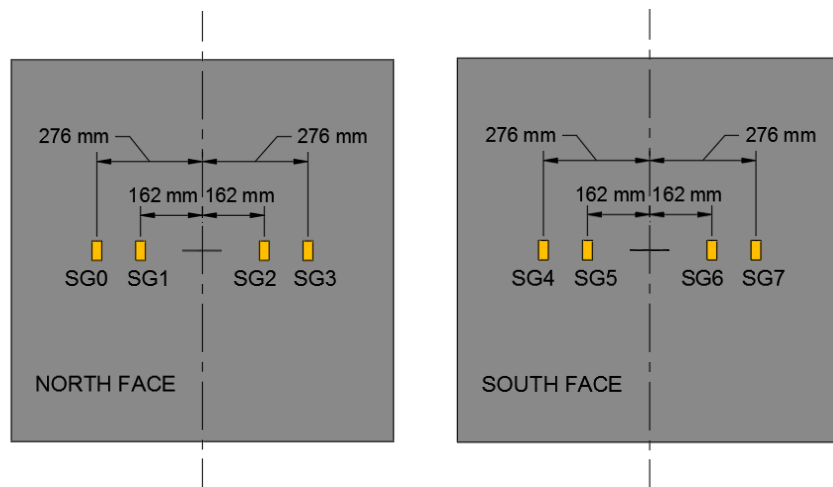


Figure 3-8. Specimen 2 strain gauge layout

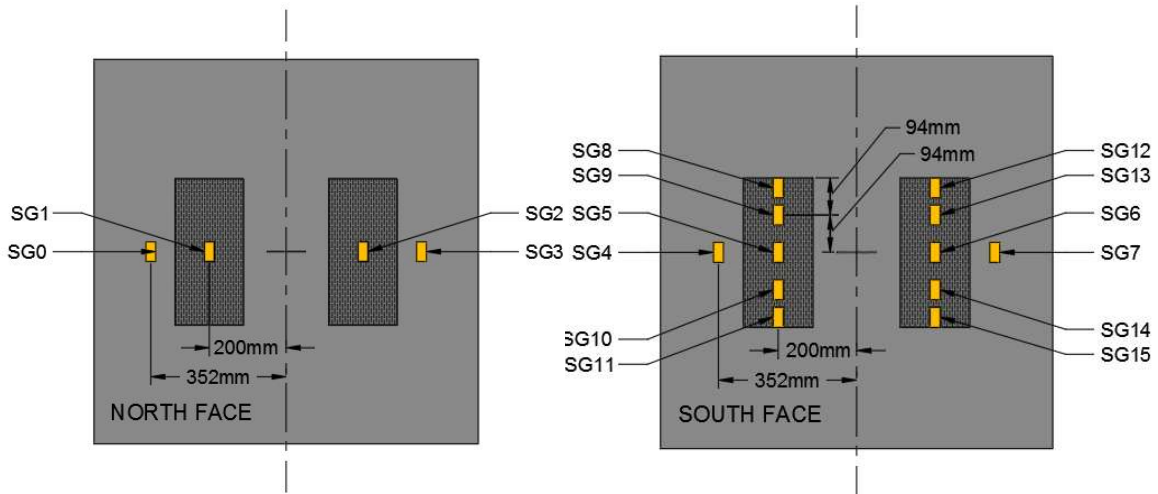


Figure 3-9. Specimen 3 strain gauge layout

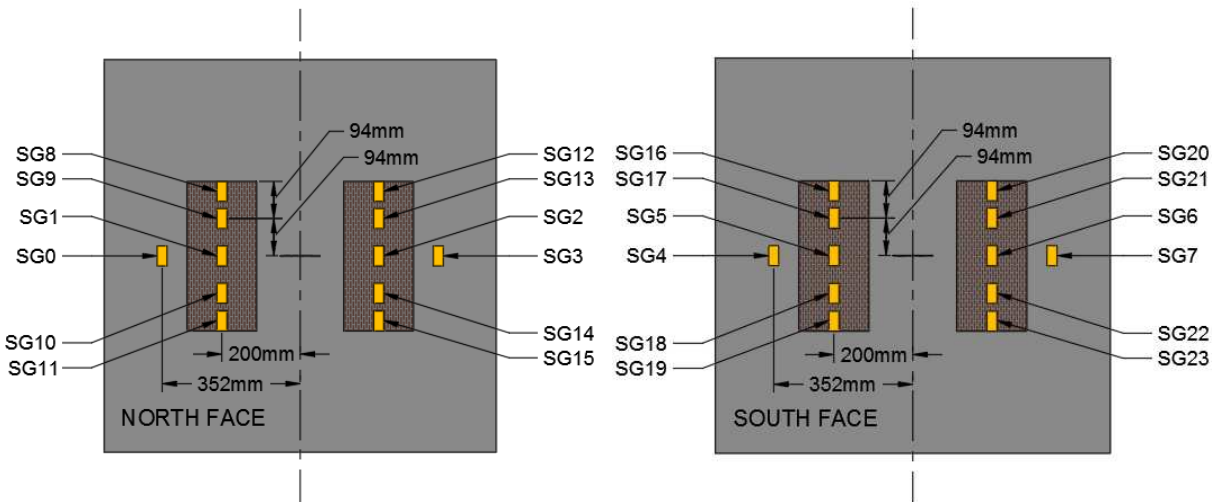


Figure 3-10. Specimen 4 strain gauge layout

3.7 Test Procedure

Specimens were subjected to a constant amplitude fatigue load with amplitude of 55 MPa (8 ksi) and frequency of 0.6 Hz. A slightly positive stress ratio of 0.1 was selected to avoid fully reversing the load on the test frame every cycle. Load commands were sent to the actuator using an MTS FlexTest controller. Force and displacement feedback were recorded by the controller. Strain data were recorded continuously throughout the tests using the data acquisition system.

At the beginning of each test, the initial crack was monitored closely to detect crack initiation. The initial crack length was taken as the out-to-out distance between the tack welds on either end of the cut crack. Crack propagation was taken to begin when a crack had initiated and grown through the tack welds. Crack length was then measured manually to the nearest 1.5 mm (1/16 in) in regular increments for the test duration.

A dye penetrant was used when measuring crack lengths to clearly identify the crack tip. Dye penetrant is a visual inspection method for detecting flaws. Typically, the dye is applied to a surface and allowed to penetrate any flaws. Then the excess dye is wiped from the surface, and a developer is applied. The developer draws out dye remaining in the flaws making their location appear clearly. In this case, the dye was instead applied during the fatigue loading, and the crack tip was identified by the dye forced out during the crack closure portion of the cycle.

For the retrofitted specimens, crack lengths were only measured when the crack tip was not beneath an FRP patch since no additional method for detecting the crack through the FRP was implemented. Visual observations of retrofit behavior were also made throughout the test to help identify any debonding behavior for comparison to that detected by the strain gauges along the length of the FRP patches.

Tests were considered complete when the crack length was such that final fracture of the specimen was imminent. Specimens were not intended to be tested to fracture because the fracture can cause a shock to the test frame, possibly altering alignment or affecting bolt pretension. Typically, the crack grew to 100 mm to 120 mm away from the specimen edge before crack growth accelerated dramatically and the test was stopped.

CHAPTER 4

EXPERIMENTAL RESULTS AND DISCUSSION

4.1 Introduction

Results from the four specimens are presented and discussed herein. Each specimen was cyclically loaded as previously described until fracture occurred or was imminent. Crack growth versus number of cycles and strain in the steel and FRP, when applicable, were recorded throughout the tests. Comparison of specimens 1 and 2 allowed for the deleterious effect of the underwater environment to be quantified. Effectiveness of the retrofit methods was determined by comparison of the repaired specimens to the unrepaired specimens. Comparison between specimen 3 and specimen 4 allowed for assessment of the use of BFRP as an alternative to CFRP.

4.2 Individual Specimen Results and Observations

During each test, crack length and the corresponding number of cycles were periodically noted, and readings from all strain gauges were continuously recorded. Crack length was measured for the east and west cracks on both the north and south faces by applying dye penetrant to make the location of the crack tip appear clearly. It was found that the cracks grew equally through the thickness of the specimens, so average values for the east and west cracks are presented for each time that measurements were taken. From the recorded strains, maximum values corresponding to the times the crack measurements were taken were noted. For unretrofitted specimens, crack growth data were used to calculate Paris Law parameters C and m for use in comparing the air and underwater environments.

Observations of the crack behavior were made for each specimen during and after the tests. After test completion, specimens that remained intact were cut along the crack plane in order to observe the characteristics of the crack face. In addition, the FRP bond was closely monitored for the retrofitted specimens. Debonding around the edges of the adhesive was detected by spraying the area with water, such that water was forced out of the gap between the adhesive and steel during the load cycle if the two were not in contact. The failure method of the FRP was observed at the end of tests of retrofitted specimens as either debonding failure, fiber rupture failure, or a combination.

4.2.1 Specimen 1

Specimen 1 was tested in air with no retrofit, as shown in Figure 4-1. In addition to the typical strain gauges applied along the crack plane for all specimens, an additional gauge was installed 100 mm above the crack plane on both faces of specimen 1 for the purpose of verifying the nominal applied stress range. The applied load range corresponds with a stress range of 55 MPa. At the beginning of the test before crack propagation, the gauges were checked and strains corresponding to stress ranges of 72 MPa and 37 MPa were recorded on the north and south faces, respectively. This indicates the presence of some level of out-of-plane bending, which was attributed to slight misalignment in the test frame. It was assumed that the stress distribution through the plate thickness was linear, so that stress range experienced at mid-thickness was 55 MPa. Despite the bending, crack growth was essentially equal on the north and south faces for specimen 1 and all other specimens.

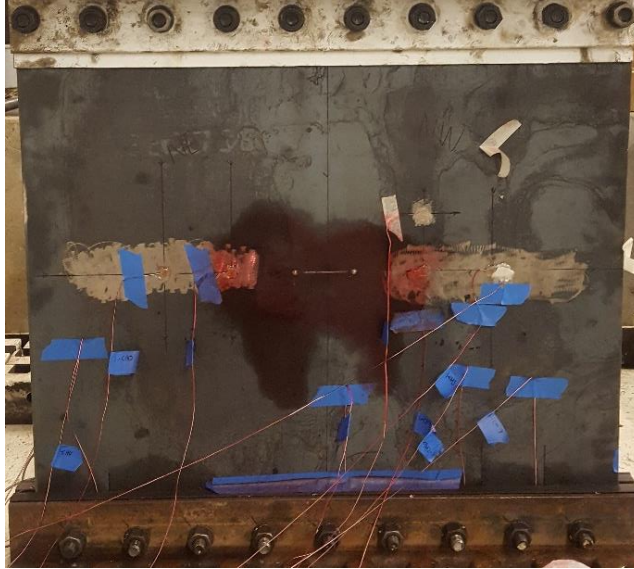


Figure 4-1. North face of specimen 1 at early stage of test

4.2.1.1 Specimen 1 Crack Growth

Cracks initiated from the tack welds at both ends of the pre-cut crack at approximately the same time. Crack propagation measurements are shown in Figure 4-2. The two crack tips propagated at similar rates until reaching a half crack length of 75 mm. After this point the west crack began to propagate more quickly than the east crack. The difference in length between the two cracks increased throughout the test. At the completion of the test, the west crack was 100 mm longer than the east crack.

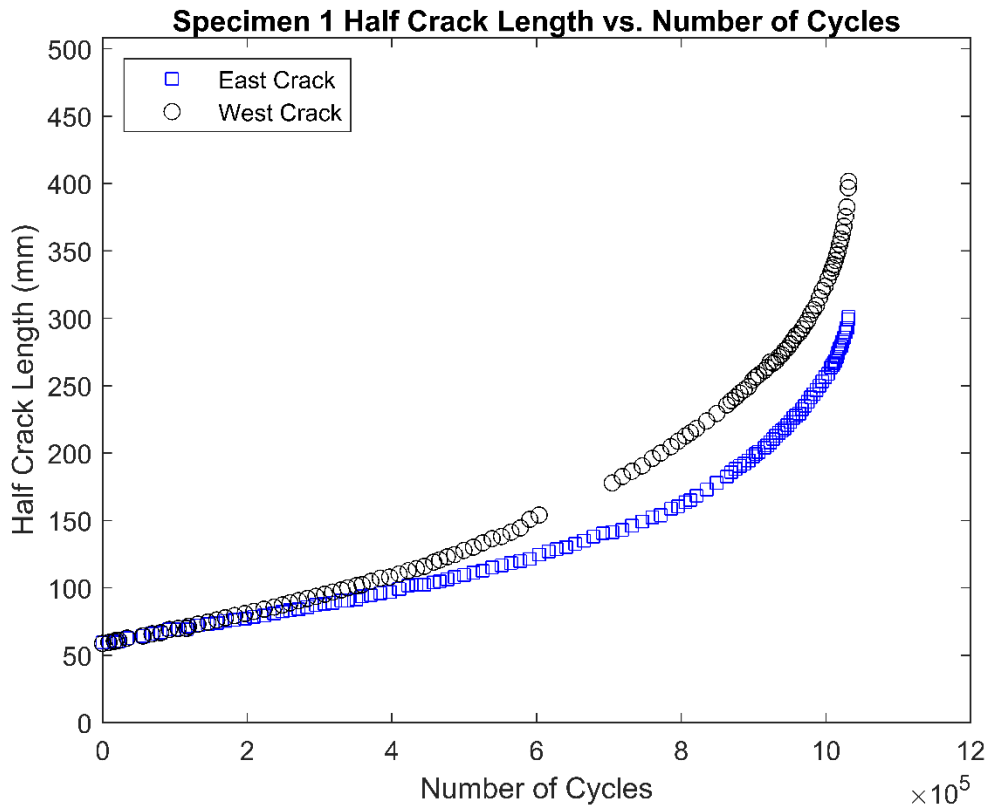


Figure 4-2. Specimen 1 crack growth measurements

The west side of the crack exhibited stable growth until a half crack length of approximately 300 mm at 975,000 cycles. The east side of the crack became unstable at a slightly lower crack length of approximately 250 mm at 990,000 cycles due to the uneven crack growth across the two sides. The test was stopped at 1,031,428 cycles when fracture of the west side was considered imminent to avoid damage to the test frame. Although fracture of the east side was not yet imminent, the east crack was showing unstable growth. The crack at the time of test completion is shown in Figure 4-3.

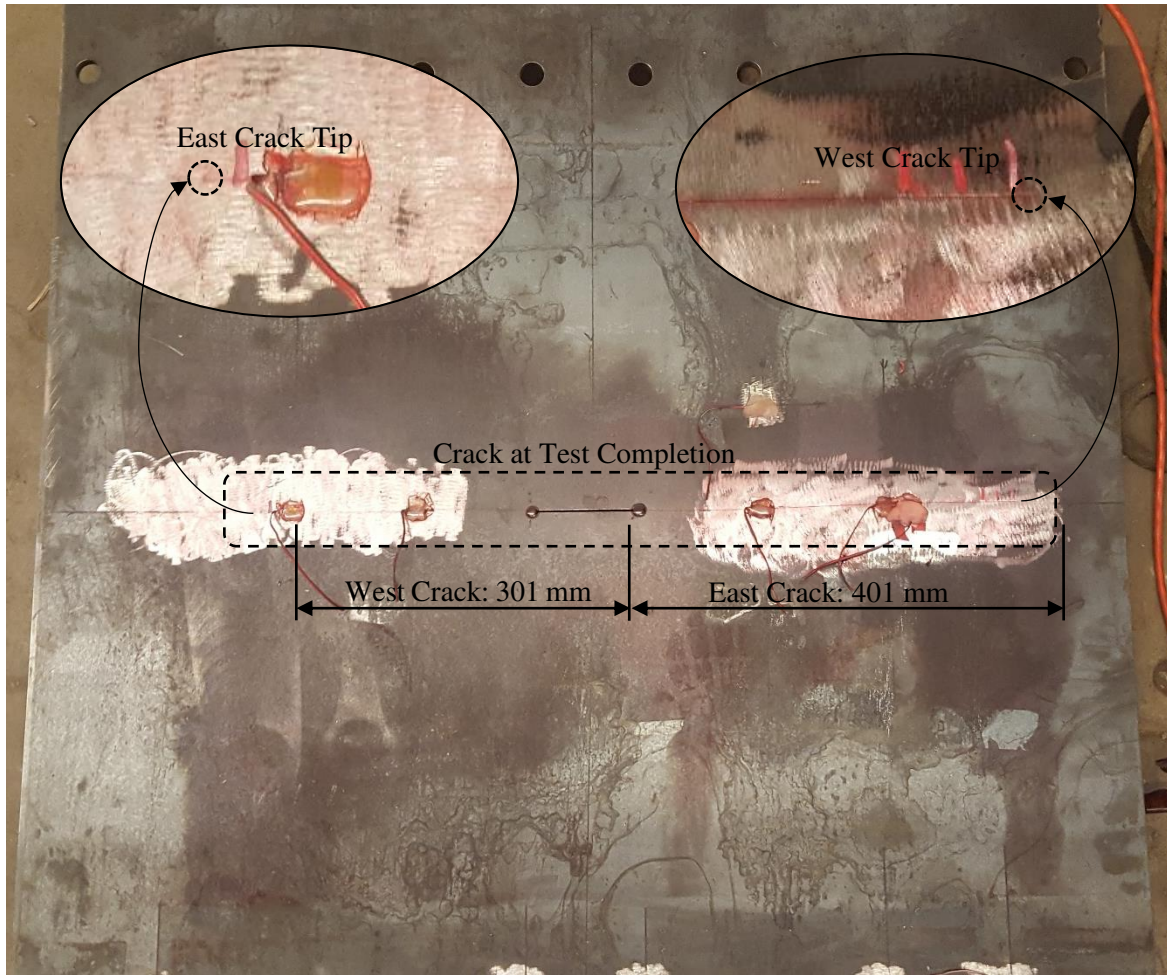


Figure 4-3. North face of Specimen 1 at test completion showing final length of east and west cracks and crack tip locations

After the test was completed, the remainder of the crack plane was cut so that the crack surface could be observed. The west crack is shown in Figure 4-4. The surface was flat, as shown in Figure 4-5, and smooth, as shown in Figure 4-4, until a half crack length of 200 mm, indicating stable growth. Between 200 mm and 300 mm, the surface began to curve as the crack growth transitioned to unstable growth. After a half crack length of 300 mm, the crack surface is clearly slanted, as shown in Figure 4-6 with a rough surface, as shown in Figure 4-4, indicating unstable growth and high ductility.

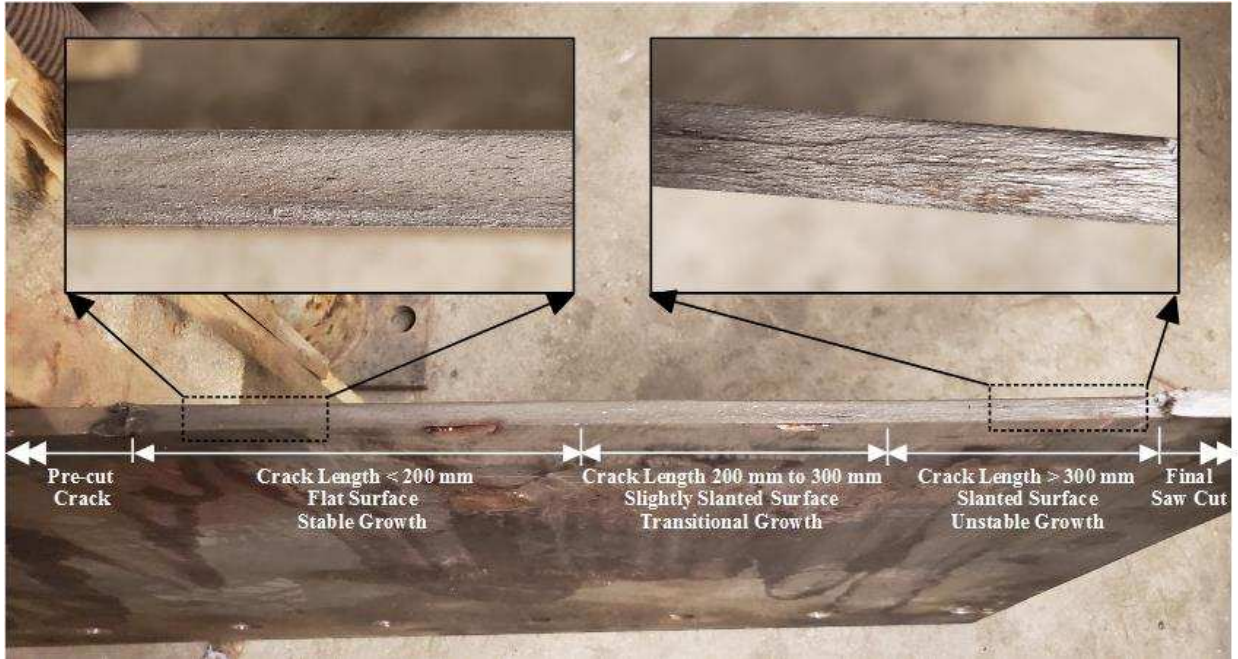


Figure 4-4. Specimen 1 west crack surface indicating transition from stable to unstable crack growth

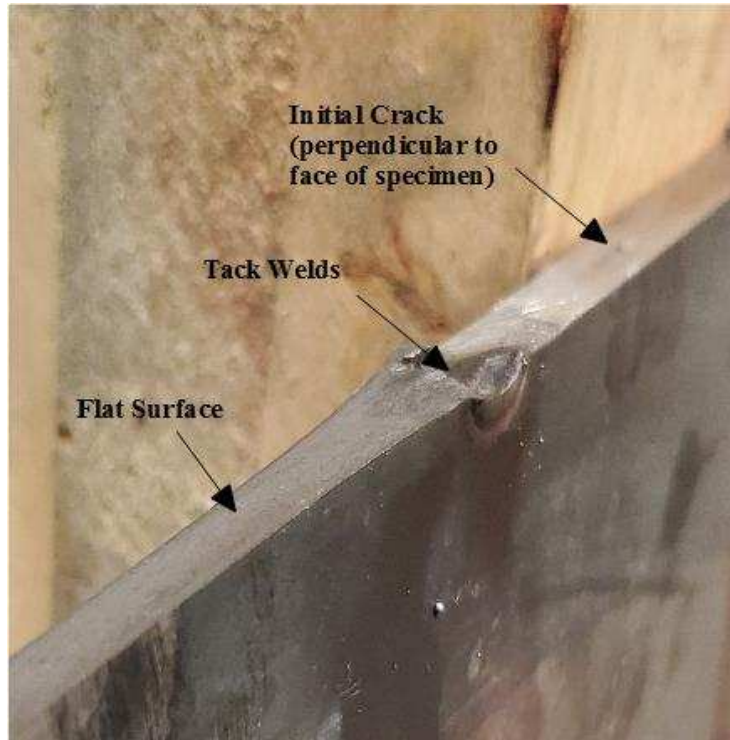


Figure 4-5. Specimen 1 west crack surface location near initial crack showing flat, smooth surface and indicating stable growth

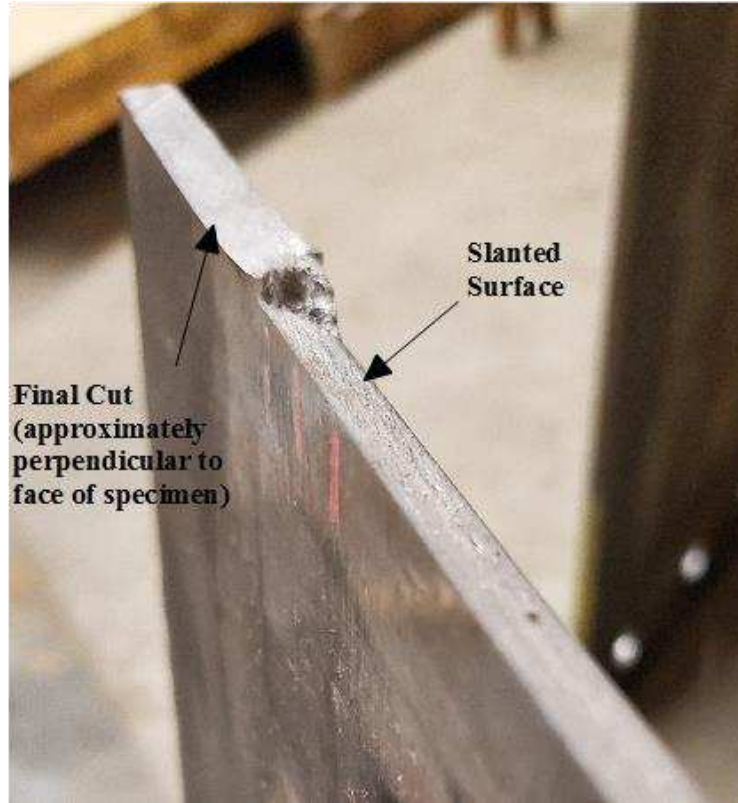


Figure 4-6. Specimen 1 west crack surface location at large crack length showing slanted surface and indicating unstable growth

4.2.1.2 Specimen 1 Crack Growth Rate and Stress Intensity Relationship

Since specimen 1 was not retrofitted, the Paris Law, which is explained in detail in Riveros et al. (2019), can be applied as a simple method for estimating the crack growth rate. Using the crack growth data acquired from testing, the Paris law parameters C and m were estimated by calculating crack growth rate (da/dN) and stress intensity factor range (ΔK). C and m are the y-intercept and slope, respectively, of da/dN versus ΔK plotted on a log-log scale, as shown in Figure 4-7. Separate parameters were calculated for the east and west crack, and resulting values are presented in Table 4-1. Calculated parameters are for crack length and stress intensity factor in units of mm and $\text{MPa}\cdot\text{mm}^{1/2}$, respectively. The first several crack length measurements were excluded from the calculation because they may have been affected by the presence of the tack

welds. Additionally, measurements taken after unstable growth was noted were excluded, as the Paris law no longer applies.

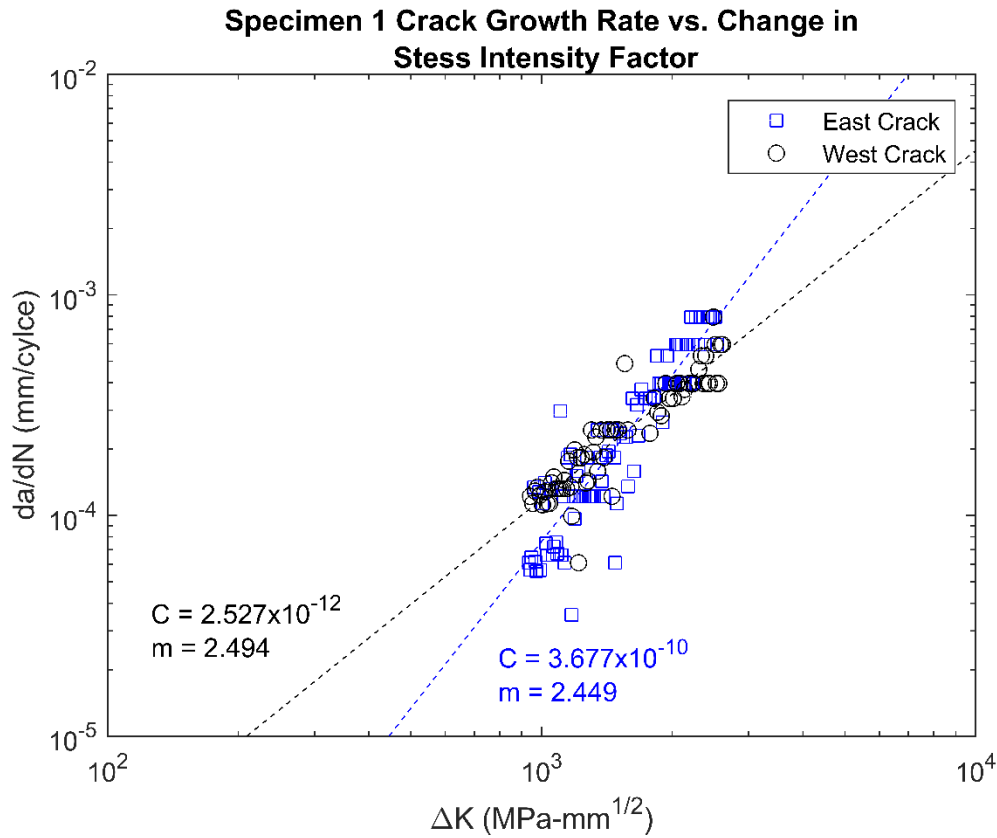


Figure 4-7. Plot of crack growth rate and stress intensity factor range for determination of Paris Law parameters for specimen 1

Table 4-1. Specimen 1 Paris Law parameters for crack growth in mm and stress intensity factor in $MPa^{1/2}$

Location	C	m
East Crack	3.677×10^{-10}	2.449
West Crack	2.527×10^{-12}	2.494

4.2.1.3 Specimen 1 Strain in Crack Plane

For strain gauges placed along the plane of crack growth, it is expected that strain readings increase as the crack length increases. As the crack tip approaches a gauge, the reading is expected

to grow rapidly, as the gauge is then located within the plastic zone around the crack tip. Results from specimen 1 shown in Figure 4-8 follow the expected behavior. The crack reached strain gauges 1 and 2 first, as they were placed closer to the center of the specimen.

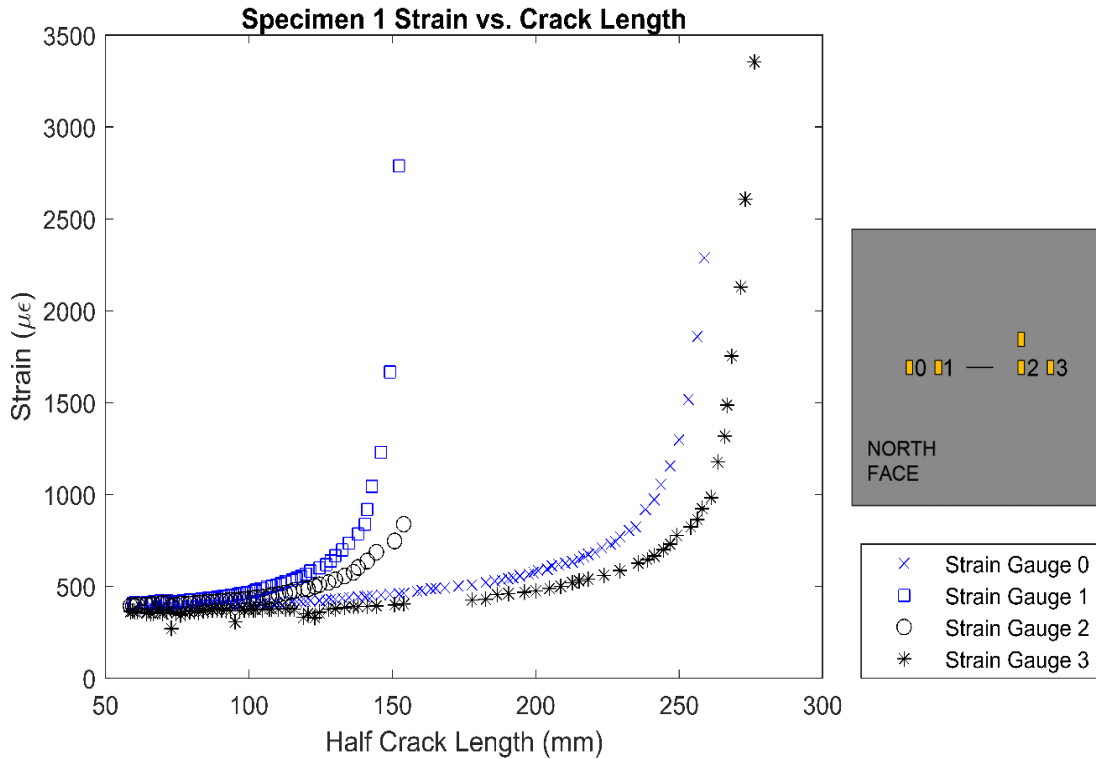


Figure 4-8. Specimen 1 strain in crack plane vs. half crack length

4.2.2 Specimen 2

Specimen 2 was tested in fresh water with no FRP repair. As Shown in Figure 4-9, specimen 2 was identical to specimen 1 aside from the addition of the water tank. Figure 4-10 shows specimen 2 in the water tank midway through the test.

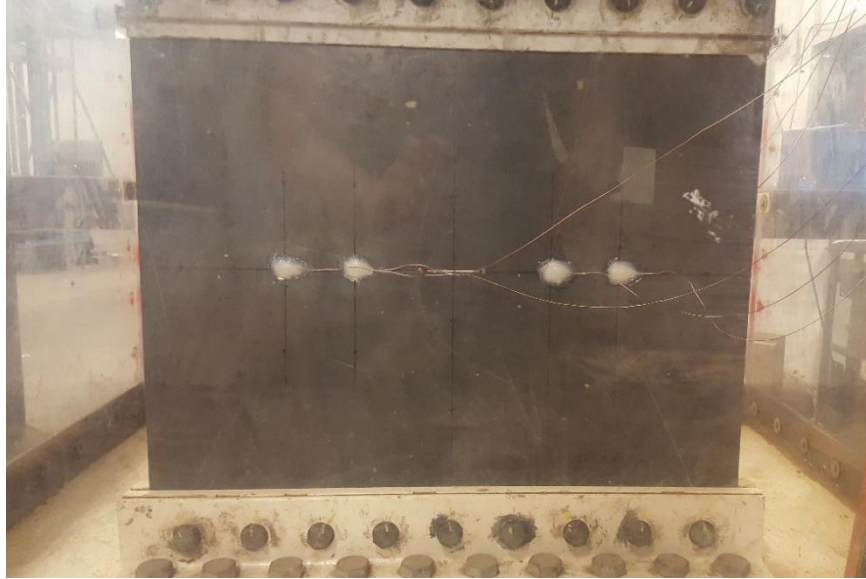


Figure 4-9. Specimen 2 before beginning test (prior to filling tank with water)

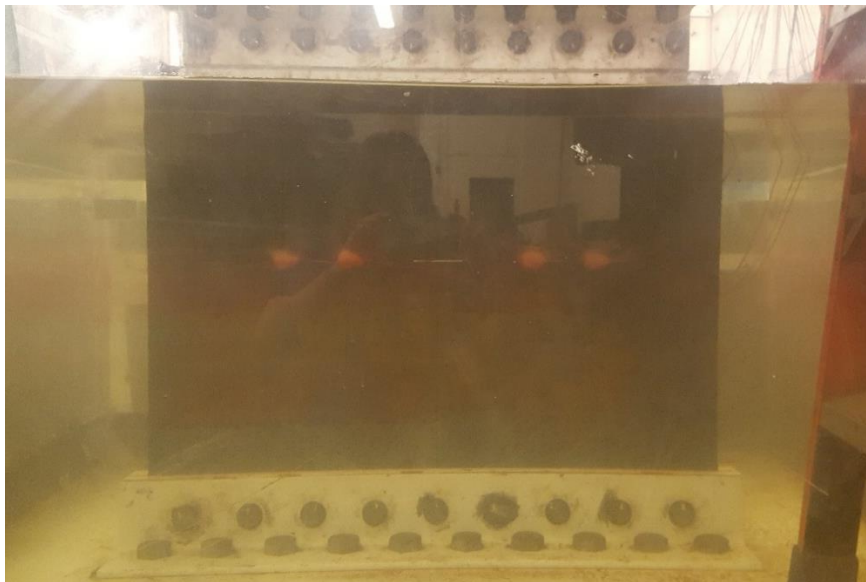


Figure 4-10. Specimen 2 underwater during test

4.2.2.1 Specimen 2 Crack Growth

Measurements of crack growth for specimen 2 are shown in Figure 4-11. Measurements were taken less frequently for the underwater specimens compared to specimen 1 due to the added time needed to drain and refill the water tank to take a measurement. Additionally, gaps in the

crack measurement data for specimen 2 are larger than specimen 1 because the silicone sealant covering the strain gauges increased the size of the blocked area beneath them.

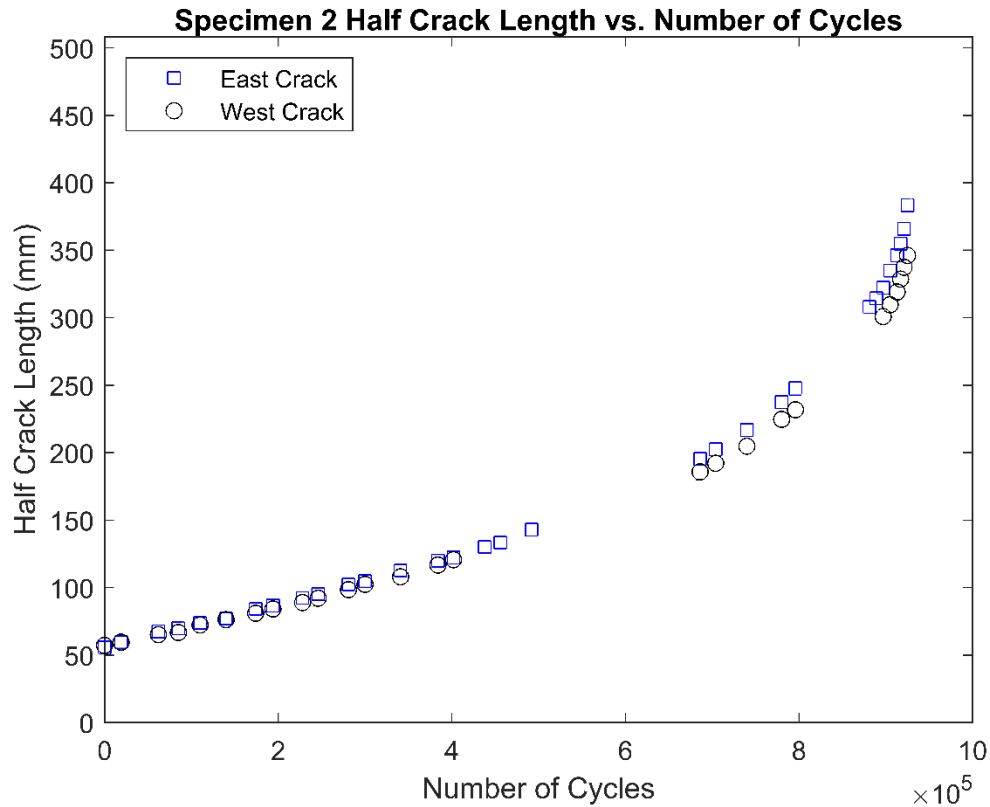


Figure 4-11. Specimen 1 Crack Growth Measurements

Cracks on the east and west sides of specimen 2 began to propagate from the tack welds at the same time. Both cracks grew equally until reaching lengths of approximately 200 mm at which point the east side began to propagate faster than the west side. At the end of the test, the east crack was approximately 40 mm longer than the west crack.

Crack growth was stable until a half crack length of approximately 300 mm. Both cracks reached 300 mm after approximately 880,000 cycles. The test was stopped at 925,000 cycles, when the crack began to grow very rapidly and fracture was imminent. Figure 4-12 shows the south face of specimen 2 after the test was completed and it was removed from the testing frame.

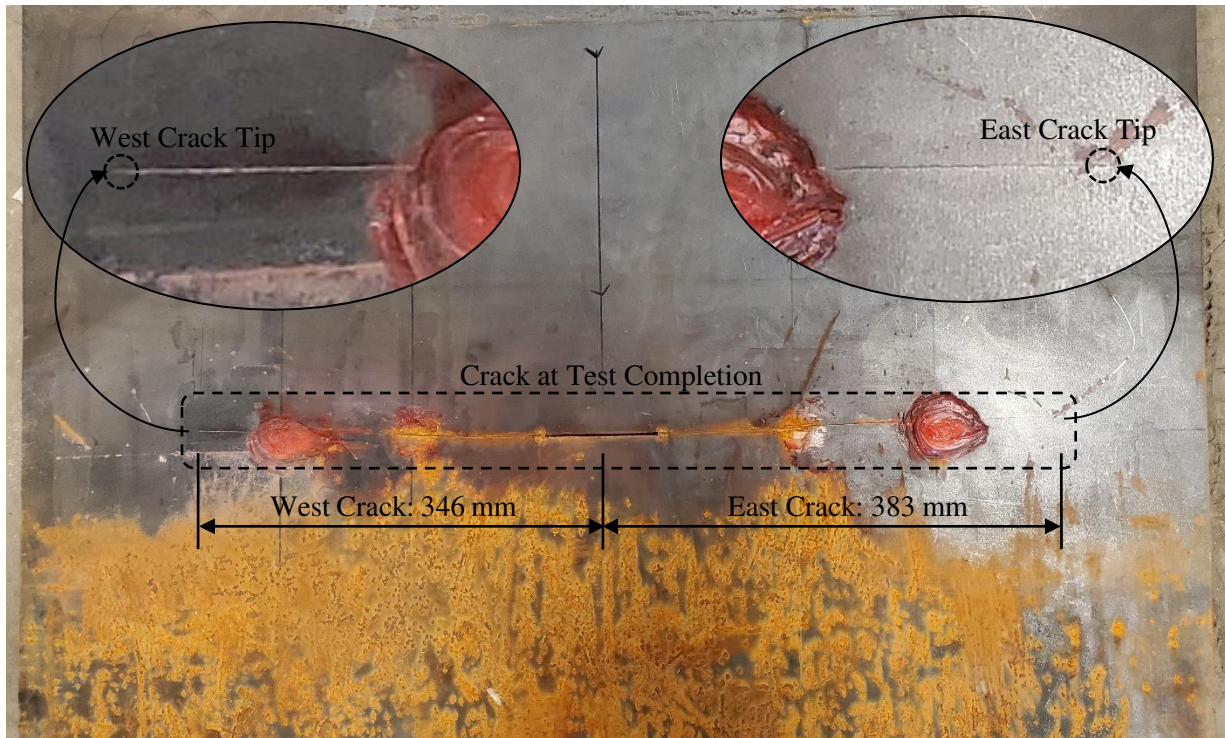


Figure 4-12. South face of specimen 2 after test completion showing final crack lengths and crack tip locations

The remainder of the crack plane was cut so that the crack surface could be observed, as shown in Figure 4-13. The surface was flat and smooth, as shown in Figure 4-14, until a half crack length of 175 mm, indicating stable growth. Between 175 mm and 300 mm, the surface began to curve as the crack growth transitioned to unstable growth. After a half crack length of 300 mm, the surface became slanted, as shown in Figure 4-15, indicating unstable growth and high ductility.

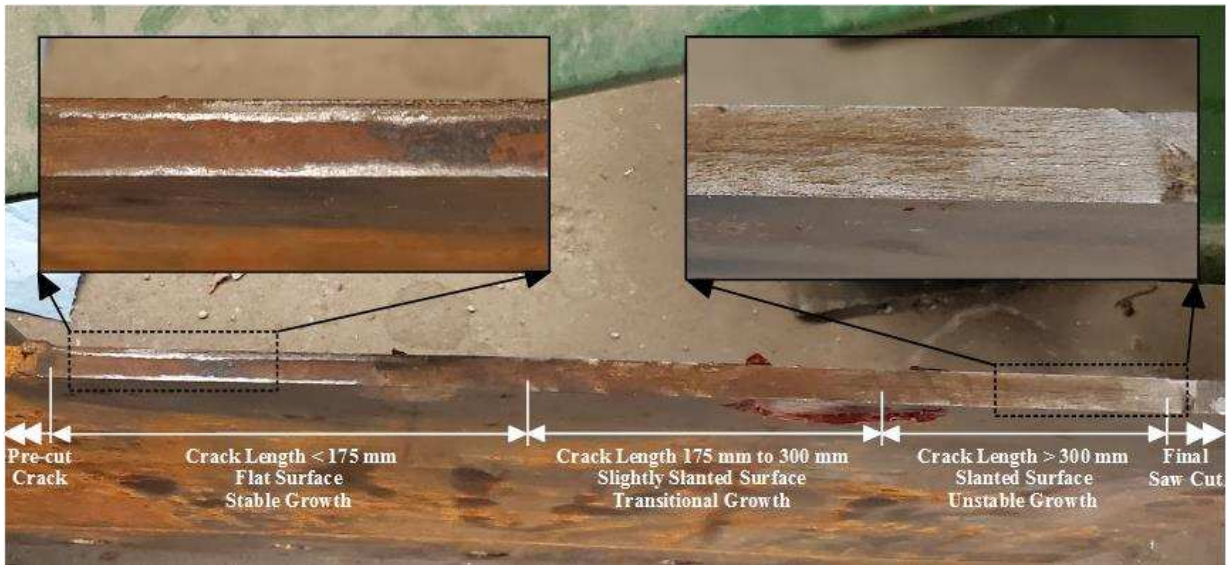


Figure 4-13. Specimen 2 east crack face showing transition from stable growth to unstable growth with increasing crack length

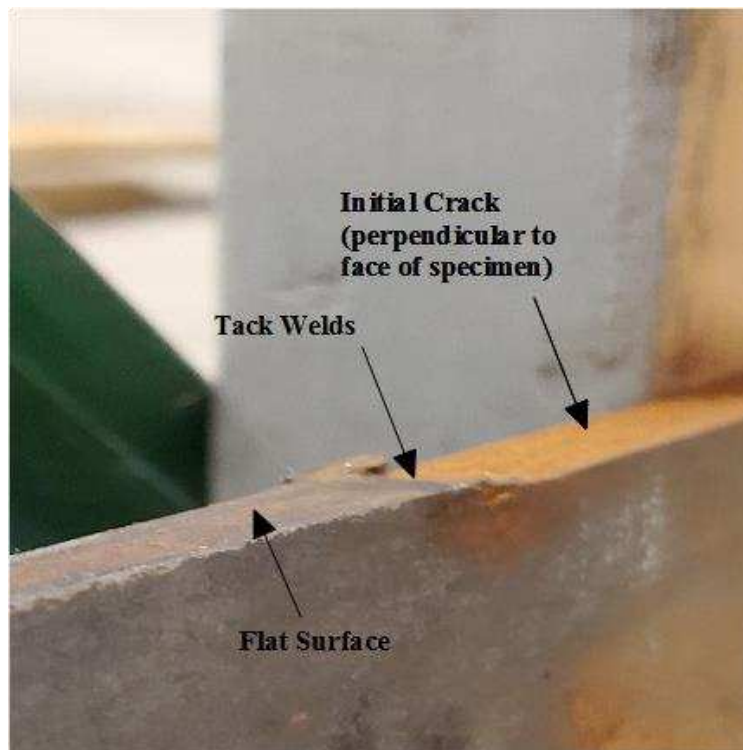


Figure 4-14. Specimen 2 east crack face location near initial crack showing flat surface and indicating stable growth

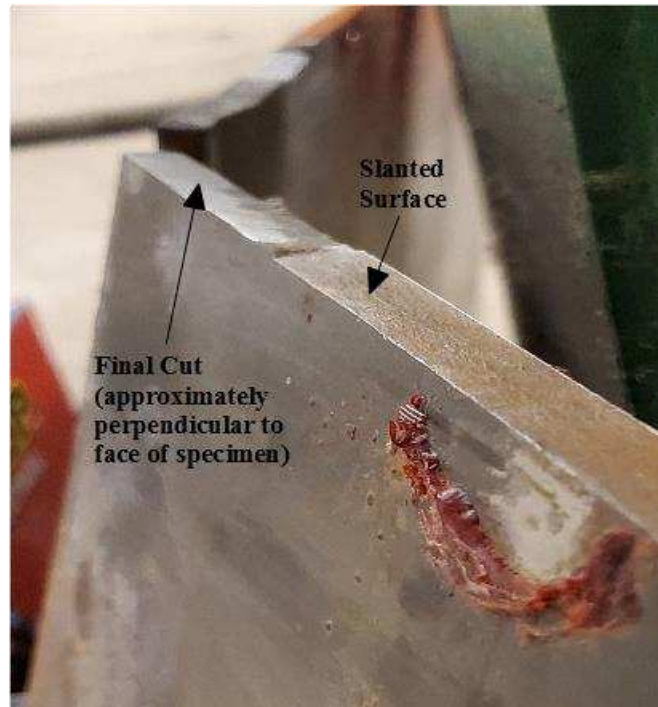


Figure 4-15. Specimen 2 east crack face location at large crack length showing slanted crack surface and indicating unstable growth

4.2.2.2 Specimen 2 Crack Growth Rate and Stress Intensity Relationship

The Paris Law parameters (C and m) were calculated for specimen 2 in the stable growth region in the same way as was done for specimen 1. Figure 4-16 shows the log-log plot used in the calculation, and resulting values are presented in Table 4-2. The results account for the underwater environment and are specific to the procedure and geometry used in the test.

Values for the parameters in fresh water are available in the literature but vary and are often not reliable due to small sample sizes. Mean values for steel in air and marine environment are provided by BS 7910 (2015) are shown in Table 4-3 for comparison to the calculated values. The marine environment values are applicable for seawater or 3% NaCl solution with frequencies between 0.17 Hz and 0.5 Hz and temperatures between 5 °C to 20 °C (BS 7910, 2015). Although the specified marine environment does not correspond directly to the tested freshwater environment, the values are considered reliable. Additionally, the difference between fatigue life

in fresh water and salt water is often not large in comparison to the difference between fresh water and air (Morgantini et al., 2018). Results in Table 4-2 and BS 7910 (2015) values in Table 4-3 indicate that the increase in parameter C and decrease in parameter m found for specimen 2 in comparison to specimen 1 are reasonable and follow the same behavior as the provided values for air and marine environment.

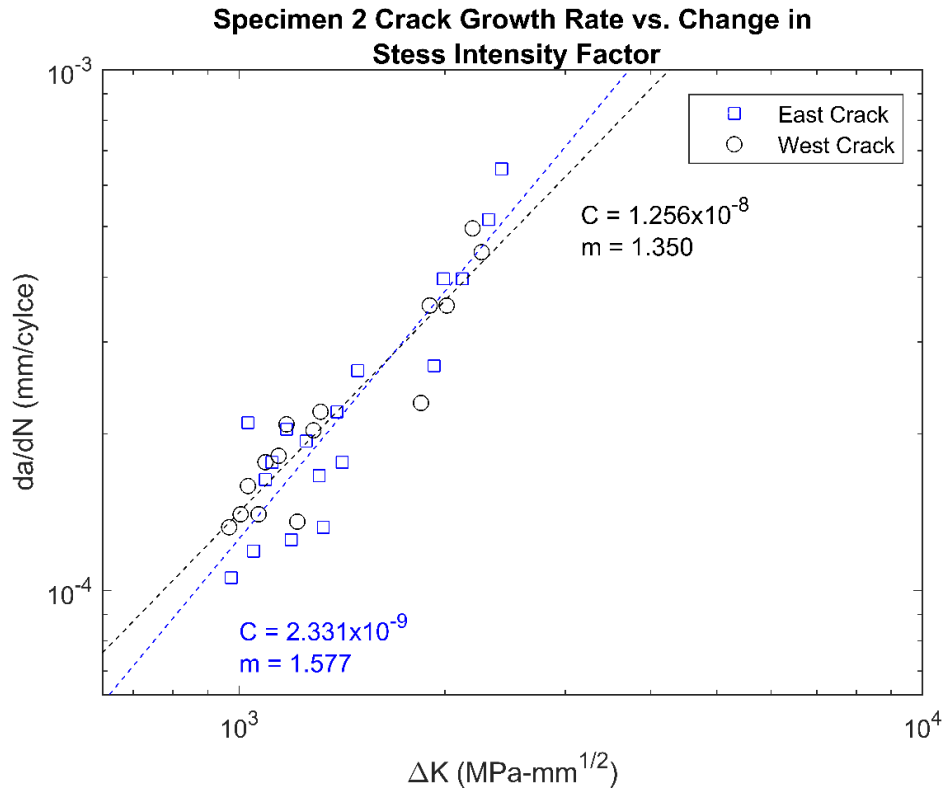


Figure 4-16. Plot of crack growth rate and stress intensity factor range for determination of Paris Law parameters for specimen 2

Table 4-2. Specimen 2 Paris Law parameters for crack growth in mm and stress intensity factor in mm- $MPa^{1/2}$

Location	C	m
East Crack	2.311×10^{-9}	1.577
West Crack	1.256×10^{-8}	1.350

Table 4-3. Paris Law parameters for air and marine environment provided by BS 7910 (2015)

Environment	C	m
BS 7910 Air	3.98×10^{-13}	2.88
BS 7910 Marine	1.27×10^{-7}	1.30

4.2.2.3 Specimen 2 Strain in Crack Plane

Four strain gauges were located along the crack plane on each face of specimen 2. For clarity, strain results from the north and south faces are plotted separately in Figure 4-17 and Figure 4-18, respectively. All strain gauges showed the expected behavior with a rapid increase in strain as the crack approached the gauge location. The rapid increases are less apparent for specimen 2 than specimen 1 because crack could not be measured as close to the strain gauges due to the additional sealant. On the north face, strain gauges 0 and 1 followed the expected trend, but showed scattered results. This may be due installation or sealing errors.

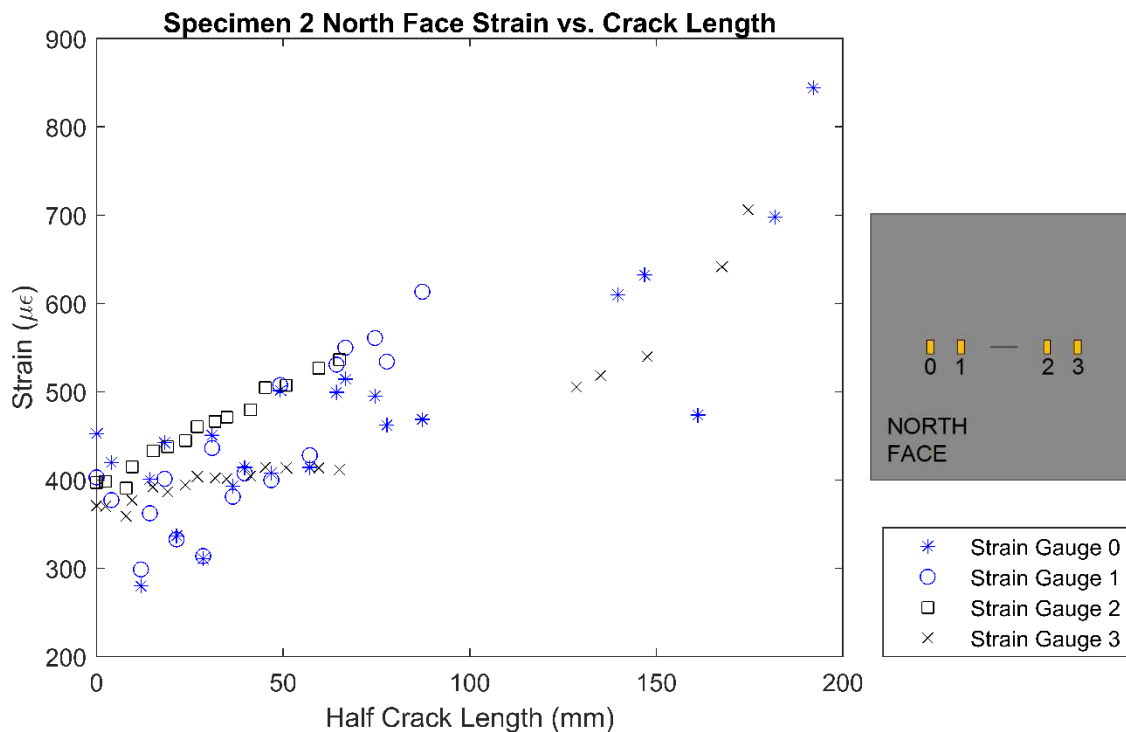


Figure 4-17. Specimen 2 north face strain in crack plane vs. half crack length

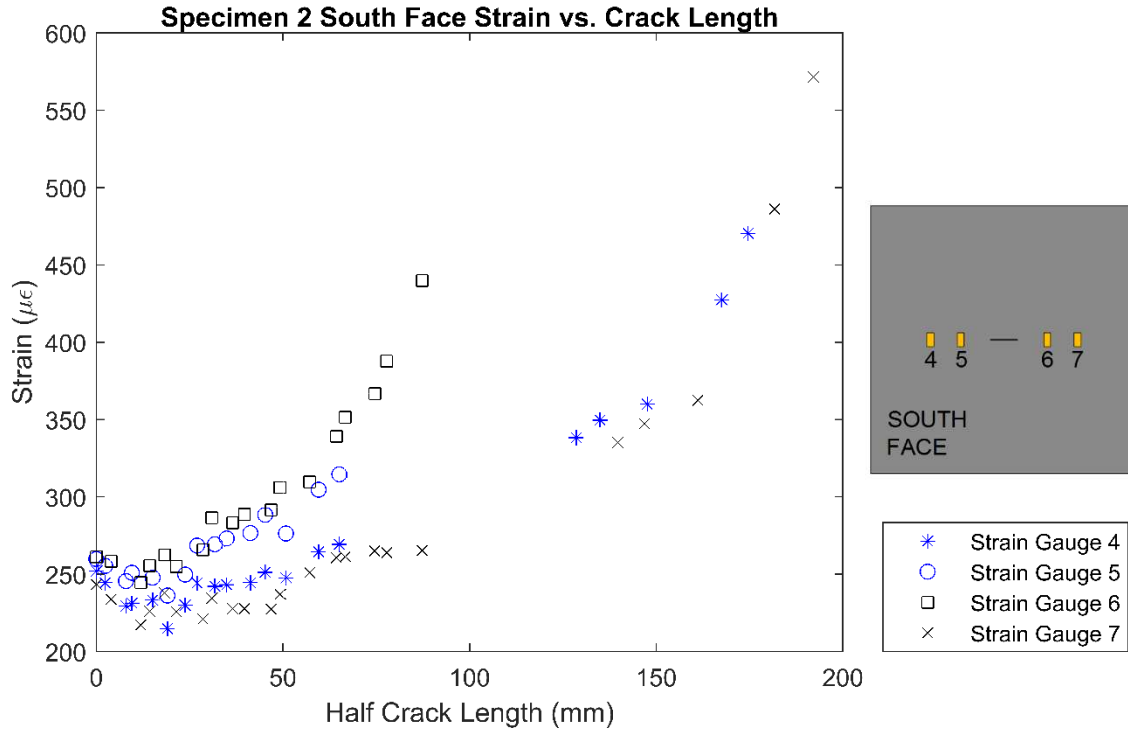


Figure 4-18. Specimen 2 south face strain in crack plane vs. half crack length

4.2.3 Specimen 3

Specimen 3 was retrofitted with two layers of CFRP on both faces and tested underwater as shown in Figure 4-19. Strain gauges, in addition to those along the crack plane, were placed along the length of the CFRP patches on the south face to detect any debonding.

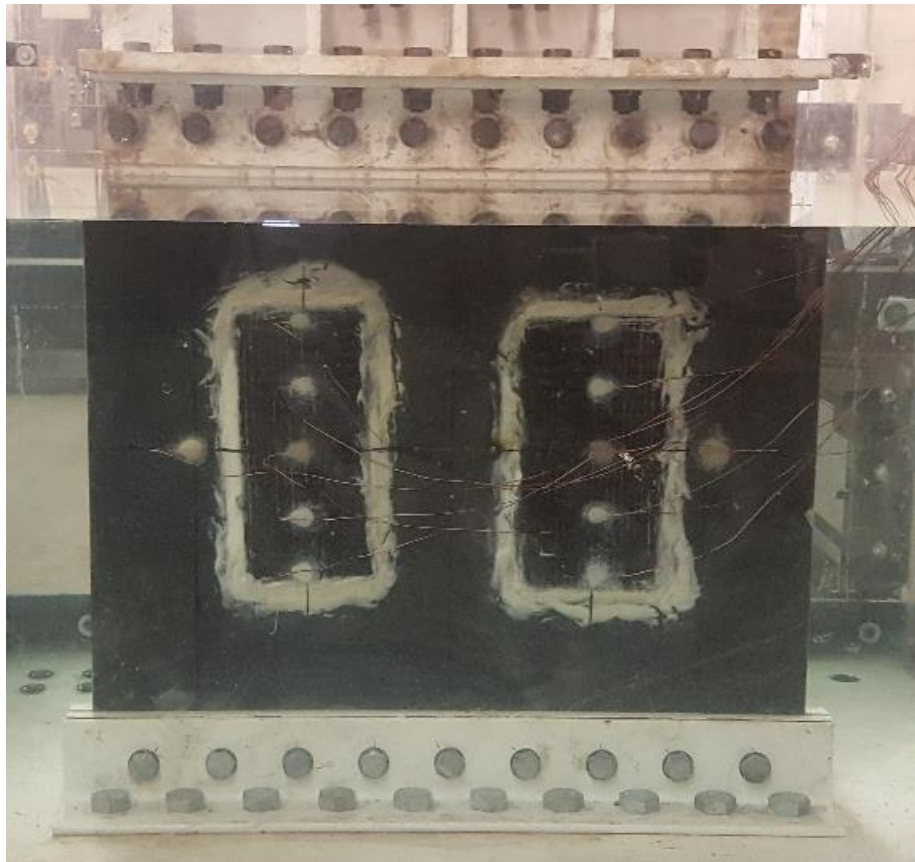


Figure 4-19. South face of specimen 3 before beginning test

4.2.3.1 Specimen 3 Crack Growth

Due to the applied CFRP retrofit, measurement of crack propagation was limited to locations where the steel was exposed for specimen 3. Cracks began to propagate on both sides of the initial crack at a similar time. Crack propagation is shown in Figure 4-20. The west side of the crack immediately began to grow more quickly than the east side. The width of the adhesive extending beyond the CFRP varied slightly at each location but was approximately 80 mm from the tack welds. The west crack reached a length of 93 mm at 380,000 cycles before reaching the adhesive. The east crack reached a length of 68 mm at 285,000 cycles and then could no longer be measured.

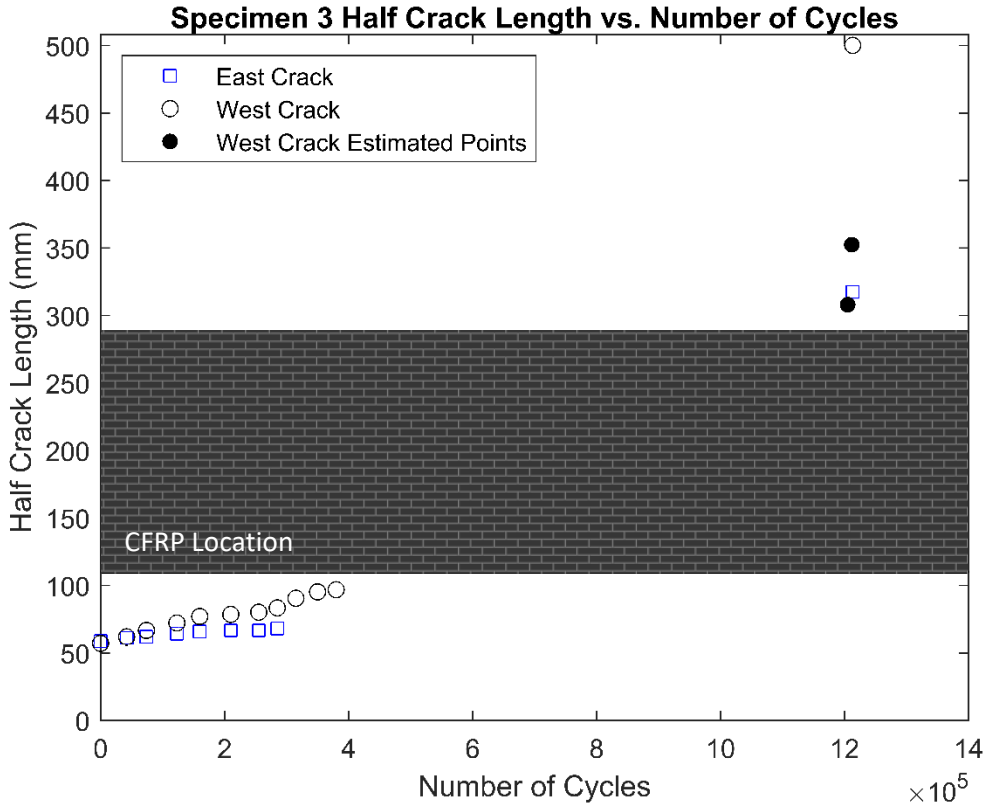


Figure 4-20. Specimen 3 crack growth measurements

When the east crack reached the adhesive, the adhesive on the north face became visibly debonded around the crack. The adhesive at the other crack tips visibly appeared to remain bonded following the cracks reaching the adhesive. On the north face of the west crack, the adhesive debonded around the crack tip at approximately 415,000 cycles. The adhesive on the south face did not appear to debond around the crack tip throughout the entire test. Debonding was also noticed along the top boundary of the CFRP patches on the north side at 380,000 cycles as is shown in Figure 4-21. By 705,000 cycles the debonding of both north patches had propagated down the top quarter of the inner edges of the patches. At 905,000 cycles, the inner edges of the north patches had debonded on the entire top half, and the outer edges had debonded on the top quarter. The edges of the entire top half of the north CFRP patches had debonded by 955,000 cycles.

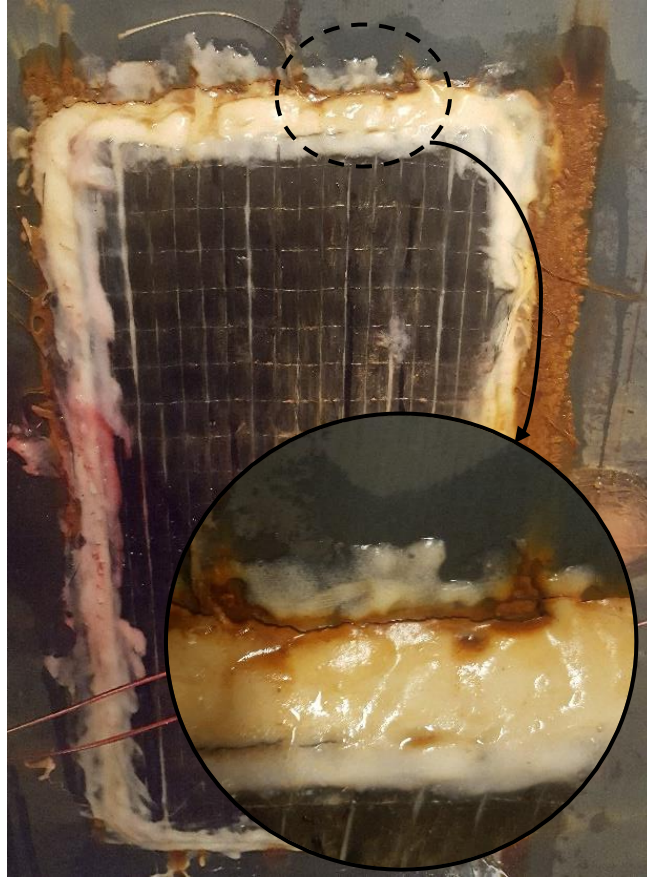


Figure 4-21. Debonding along edge of CFRP patch

Based on the results of the previous tests, it was expected that the crack would become visible again beyond the outer edge of the CFRP before fracture such that several more measurements could be recorded. However, the west crack was not observed beyond the CFRP before it fractured at 1,213,070 cycles. The east side of the crack did not fracture at the same time, and its final length was measured after the west side fractured. The north and south faces of specimen 3 after fracture are shown in Figure 4-22 and Figure 4-23, respectively. Because of the lack of crack length measurements near the end of the test, two additional measurements were estimated for the west crack, and they are denoted with solid markers on Figure 4-20. The first estimated point was taken as the outer edge of the CFRP adhesive at the number of cycles when the specimen was last inspected for a crack at that location. Another point was estimated by finding

the maximum strain recorded by the gauge in the crack plane outside of the CFRP and assuming that was when the crack passed under it.



Figure 4-22. North face of specimen 3 after fracture



Figure 4-23. South face of specimen 3 after fracture

When the specimen fractured, the CFRP on the north side remained adhered to the steel below the crack and was entirely debonded above the crack as shown in Figure 4-24. On the south face, there was no visibly detectable debonding, and fiber rupture was observed, indicating that

the full strength of the CFRP was reached. The west patch on the south face ruptured through the entire cross-section directly over the crack as shown in Figure 4-25. Fibers in the east patch on the south face ruptured but not directly over the crack as shown in Figure 4-26. The better bond behavior on the south face of the specimen may be attributed to the bending in the specimens mentioned earlier. The north face experienced a higher stress, causing more debonding. This suggests that there may be a threshold stress at which the adhesive will not debond below.

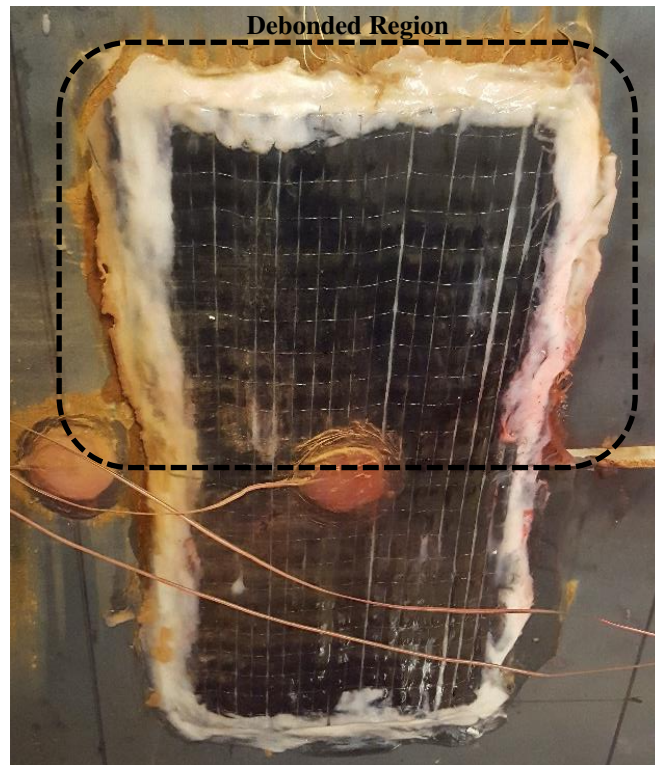


Figure 4-24. CFRP patch on north side of specimen three with top half debonded after steel fracture



Figure 4-25. CFRP fracture of west patch on south face of specimen 3

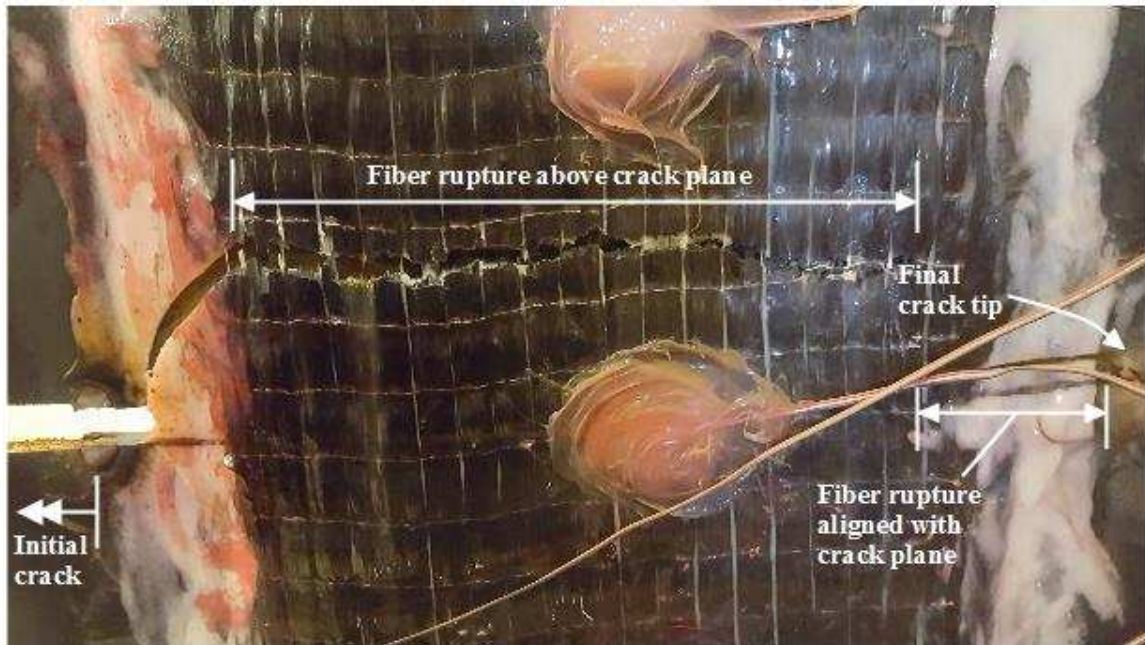


Figure 4-26. CFRP fracture of east patch on south face of specimen 3

4.2.3.2 Specimen 3 Strain in Crack Plane

Strain gauges applied on the steel were located along the crack plane, and readings corresponding to measured crack lengths are shown in Figure 4-27. For the retrofitted specimens,

the strain in steel in the crack plain is expected to show similar behavior to that of unrepaired specimens. Strain should increase gradually, although it should be slightly lower for the repaired specimens, and it should increase rapidly as the crack tip reaches the gauge. For specimen 3, the gauges located on the east side of the specimen followed this trend, but the crack did not reach all the way to the gauges before the west side fractured, meaning that the maximum strain that would have occurred when the crack tip reached the gauges was not recorded. Strain gauges on the west side showed a slight increase as the crack approached, but no rapid increase in strain occurred. As the west crack grew, it curved slightly upward such that its path was above the strain gauges rather than directly through them, so the elevated strain at the crack tip could not be observed.

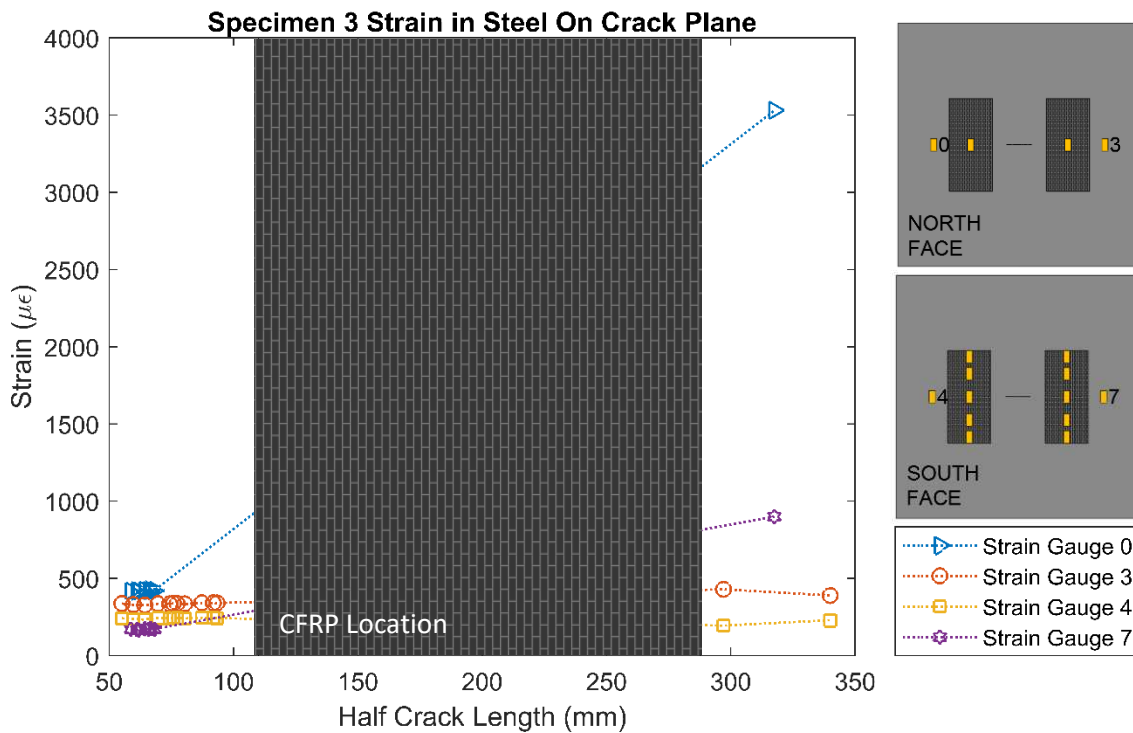


Figure 4-27. Specimen 3 strain in steel on crack plane

4.2.3.3 Specimen 3 Strain in CFRP

Strain gauges on the CFRP were located along the crack plane on both faces and along the height of the patches on the south face. The gauges on the CFRP patches were intended to assist with detecting debonding from the steel. A decrease in strain at a single strain gauge would indicate debonding at its location. However, the patches on the south face remained intact throughout the tests. Due to the limited crack length data available from the east crack, strain results from the west half of the specimen are used in Figure 4-28. to observe the CFRP behavior. Only the strain gauge that was located on the north side of the specimen showed decreasing values throughout the test. This aligns as expected with the visually observed debonding on that face. All the strain gauges on the south face recorded increasing strains throughout the test, indicating that they remained well bonded. Therefore, the south patches were bridging the crack and providing a crack closure effect until they ruptured.

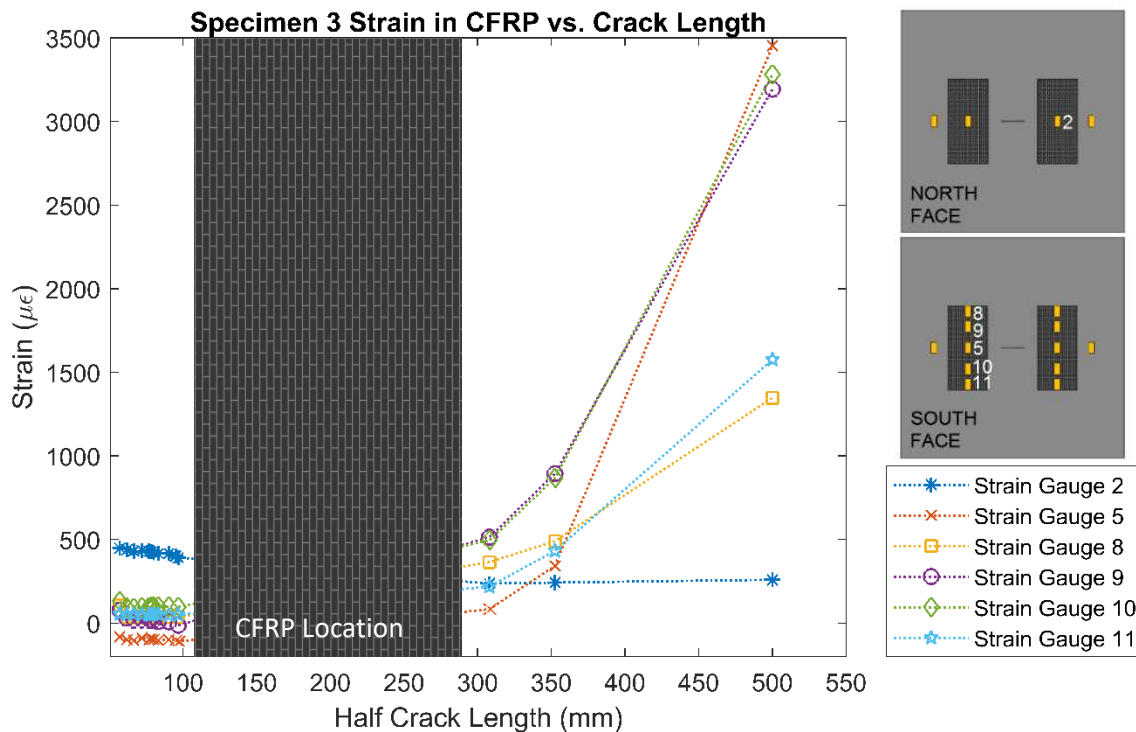


Figure 4-28. Specimen 3 west half strain in CFRP

4.2.4 Specimen 4

Specimen 4 was retrofitted with two layers of BFRP on both faces and tested underwater as shown in Figure 4-29. Strain gauges, in addition to those along the crack planes, were placed along the length of the BFRP patches on both faces to assist in detecting any debonding.

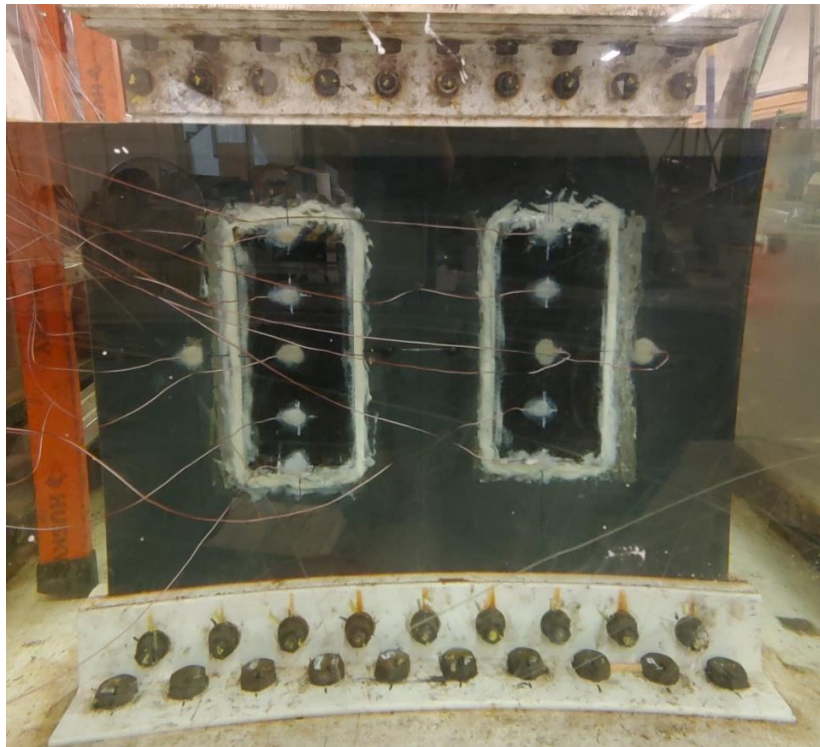


Figure 4-29. North face of specimen 4 before beginning test

4.2.4.1 Specimen 4 Crack Growth

For specimen 4, measurement of crack propagation was again limited to locations where the steel was exposed. Cracks began to propagate on both sides of the initial notches at the same time. Crack propagation results are shown in Figure 4-30. The width of the adhesive extending beyond the BFRP varied slightly at each location. The length of the west crack was 98 mm at 402,000 cycles before reaching the adhesive. The east crack reached a length of 87 mm at 402,000 cycles and then could no longer be measured.

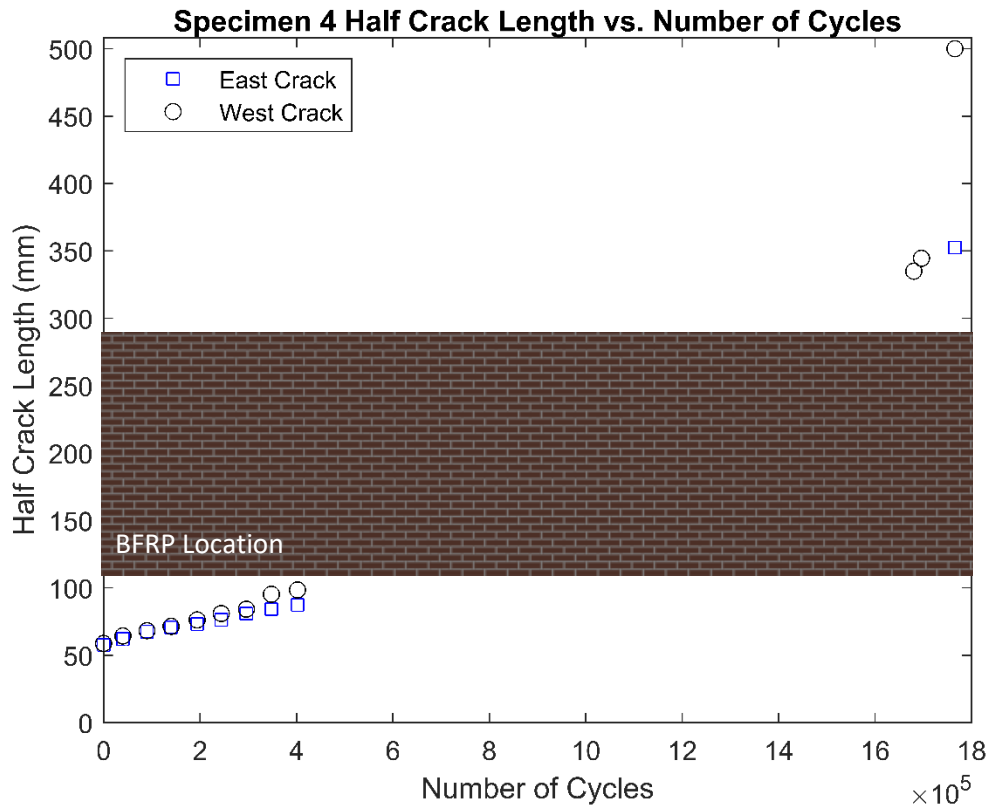


Figure 4-30. Specimen 4 crack growth measurements

After 510,000 cycles, just after the crack tips began to propagate under the BFRP patches, slight debonding became visible directly adjacent to the cracks. Debonding around the crack did not appear to propagate significantly along the vertical inside edges of the patches throughout the test. No visibly detectable debonding of the patch ends occurred throughout the entire test.

At 1,680,100 cycles, the west crack, with a length of 275 mm, appeared beyond the BFRP patch. Once beyond the patch, the west crack grew quickly until it fractured at 1,765,458 cycles. The east crack was not visible beyond the BFRP patch until the final fracture of the west half, at which point it was approximately 20 mm beyond the adhesive fillet. Figure 4-31 and Figure 4-32 show the north and south faces, respectively, of specimen 4 after fracture. Half of each BFRP patch (either the half above or the half below the crack plane) experienced failure of the adhesive bond

to steel at the time of fracture. Bond failure in all patches was similar to that shown in Figure 4-33, which illustrates the bond failure in the southwest BFRP patch. It is worth noting that this bond failure was attributed to deformation caused by out-of-plane bending of the specimen once fracture occurred.

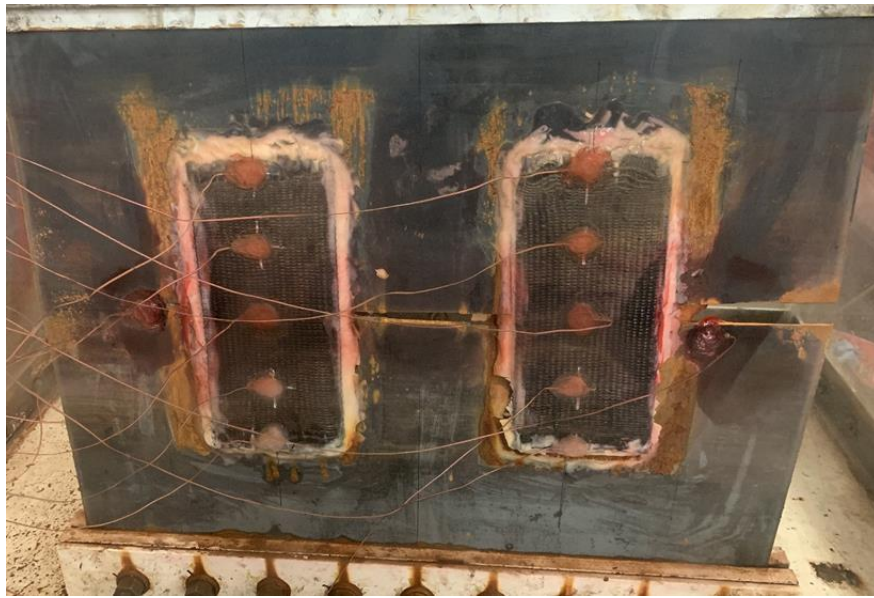


Figure 4-31. North face of specimen 4 after fracture of west crack



Figure 4-32. South face of specimen 4 after fracture of west crack

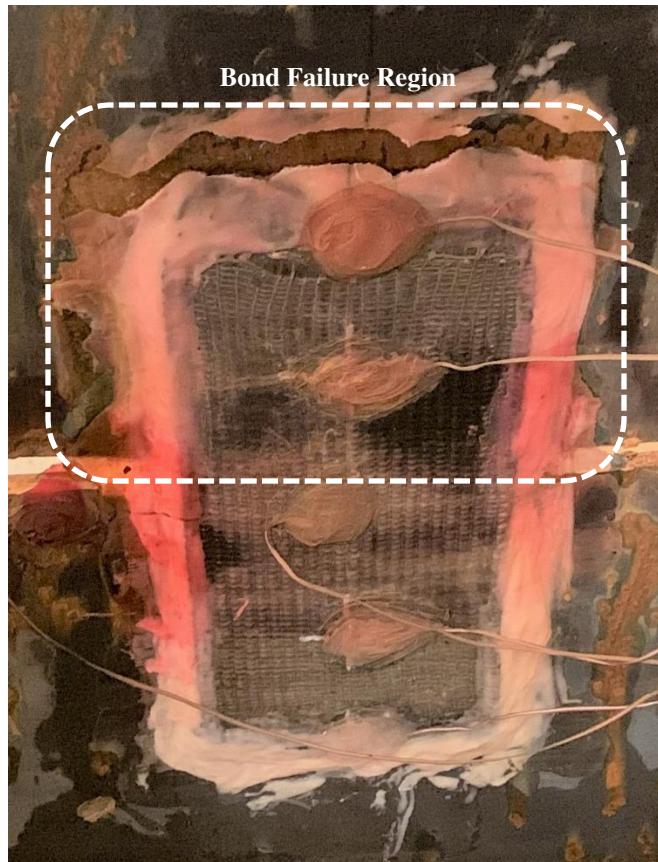


Figure 4-33. Bond failure on upper half of southwest BFRP patch

4.2.4.2 Specimen 4 Strain in Crack Plane

Strain gauges applied on the steel were located along the crack plane, and readings corresponding to measured crack lengths are shown in

Figure 4-34. A rapid increase in the readings from strain gauges 3 and 4 along the west was recorded after the crack length was beyond the BFRP. However, the elevated values are not as high as those recorded for other specimens because the crack grew slightly above the strain gauges, so maximum strains right at the crack tip were not obtained. The east crack approached strain gauges 0 and 4 just as the fracture of the west half occurred, and increased values were recorded at that instance.

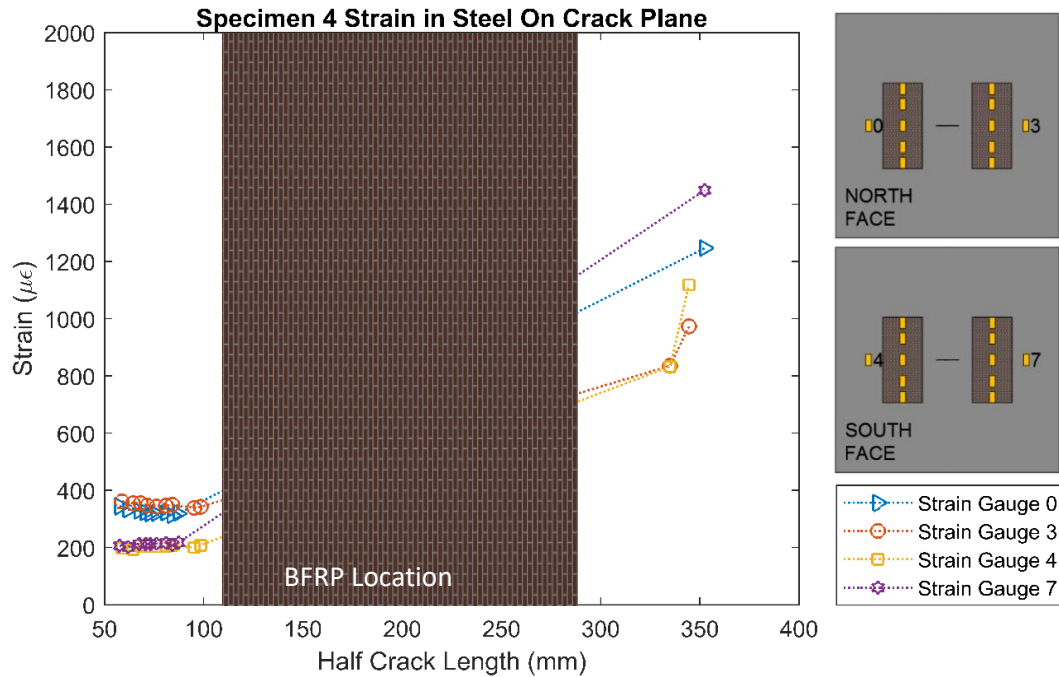


Figure 4-34. Specimen 4 strain in steel

4.2.4.3 Specimen 4 Strain in BFRP

Strain gauges on the BFRP were located along the height of the patches on both faces to assist in detecting debonding. Results for the west patch on the north face are shown in Figure 4-35. Those for the west patch on the south face are shown in Figure 4-36. Both patches on the east half of the specimen showed similar results to those from the west patch on the same face.

The strain in the gauges located in the center of the patches directly over the crack plane increased as the cracks propagated under the patches. Readings from the patch ends, such as those from gauges 12, 15, 16, and 19 as shown in Figure 4-35 and Figure 4-36, decreased as the crack propagated under the patches, indicating some bond deterioration may have occurred although it was not visibly detectable. However, the same gauges at the patch ends did still record increased values when the crack became very large and the patches began to carry more of the applied stress, indicating that while possibly deteriorated, the bonds remained intact at patch ends.

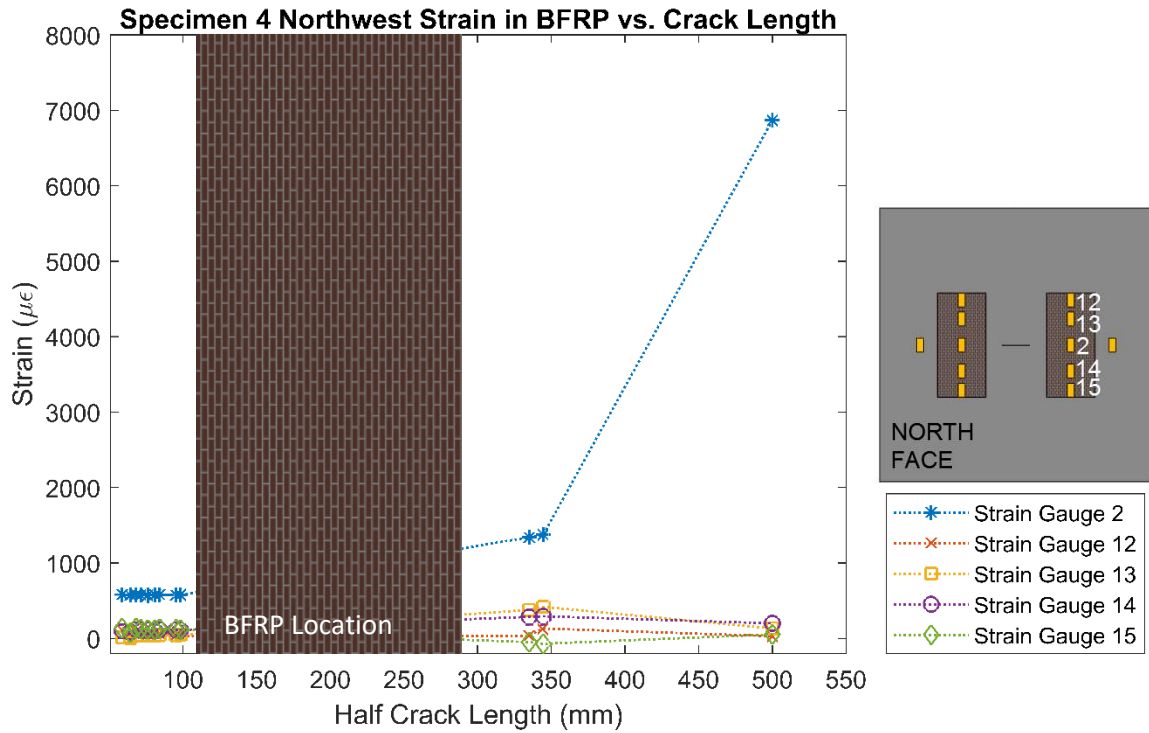


Figure 4-35. Specimen 4 strain in northwest BFRP patch

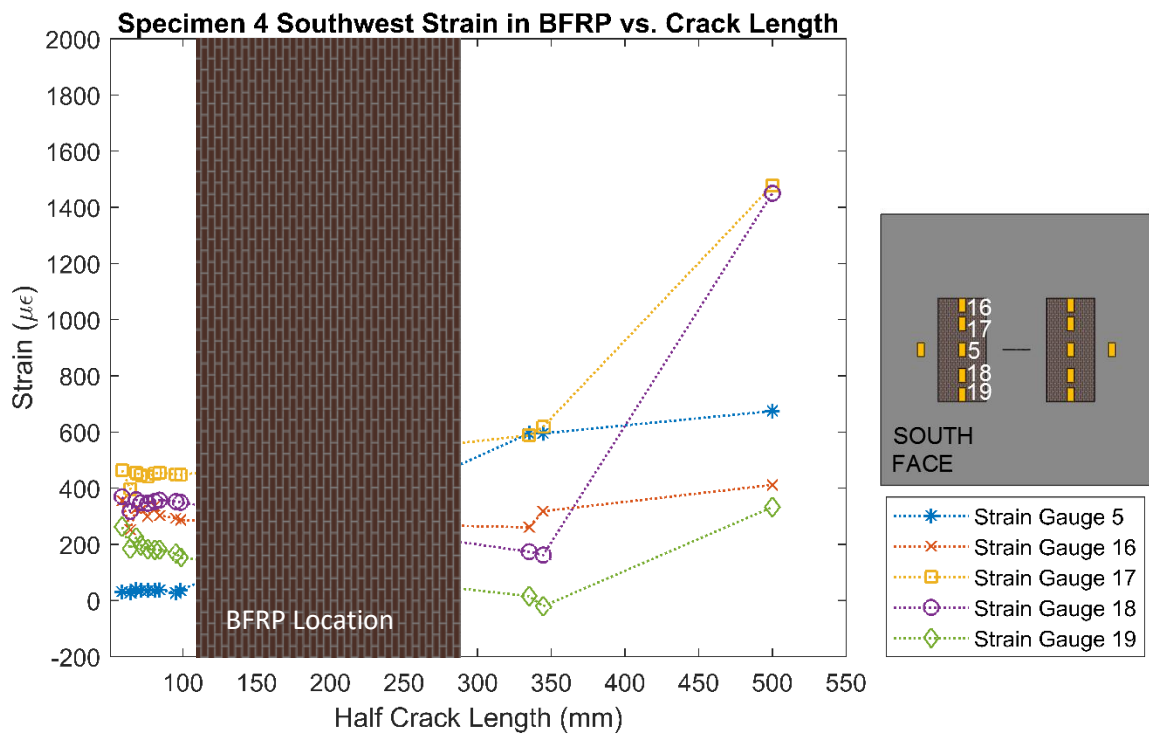


Figure 4-36. Specimen 4 strain in southwest BFRP patch

4.3 Comparison of all Specimens

Fatigue life was used as the primary metric for comparing results across specimens and determining effectiveness of the retrofits. As expected, both retrofit methods improved fatigue life, and the underwater environment reduced fatigue life in comparison to fatigue in air. Crack growth data for all specimens are shown in Figure 4-37. Specimens were also compared in pairs to identify key outcomes of the experimental program. For visual clarity and to provide an illustration of behavior behind FRP patches, estimated crack growth curves for specimens 3 and 4 are included as dashed lines in Figure 4-34 and later crack growth comparison plots. Stress intensity factors were calculated for an unrepaired specimen and then scale factors specific to each crack were used to reduce each stress intensity factor value to account for the FRP repair. Scaled values were used in the Paris Law with the parameters found from specimen 2 to obtain crack growth estimates only under the patches.

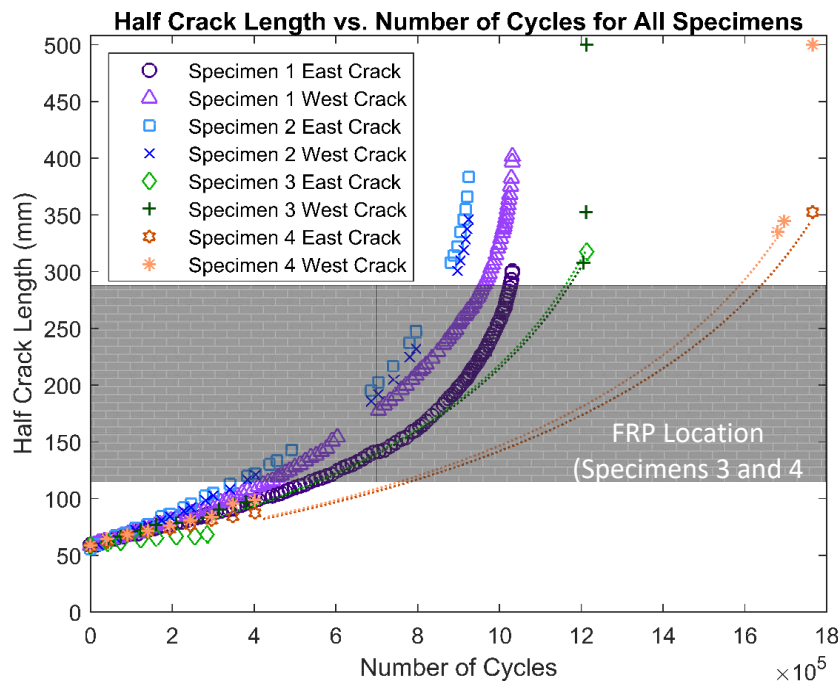


Figure 4-37. Comparison of crack growth for all specimens

4.3.1 Comparison of Specimens 1 and 2

Comparing specimens 1 and 2 allowed for the environmental effects on the steel panel alone to be quantified. The introduction of fresh water for specimen 2 reduced the fatigue life by 10.3% compared to specimen 2. Results for specimens 1 and 2 are shown together in Figure 4-38.

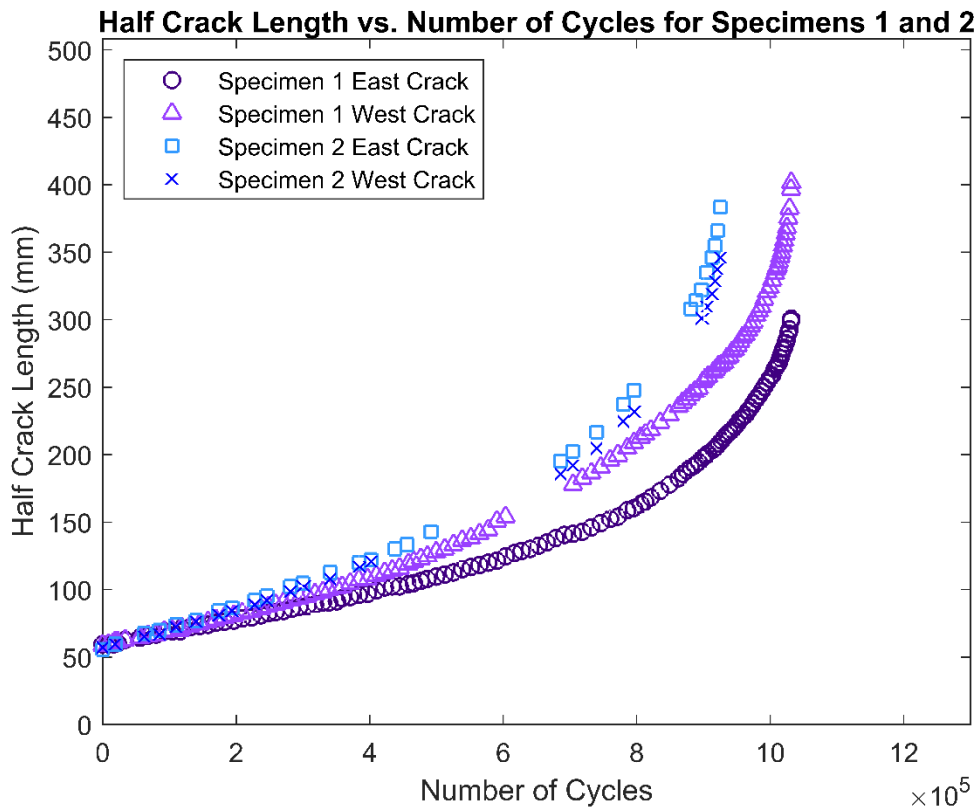


Figure 4-38. Comparison of crack growth for specimens 1 and 2

The reduced life when underwater is expected considering the mechanisms described in Chapter 2. As was also previously described, the life reduction caused by an underwater environment can vary greatly and requires the consideration of more factors than fatigue in air. Here, the reduction in life is moderate. There is a clear reduction in life but it is less dramatic than some results reported by others, such as the reduction of over 50% reported by Morgantini et al. (2018). When comparing the Paris Law parameters calculated for the two specimens, the values

are also clearly reduced when underwater. It should be noted that, because of the large scatter typical of fatigue results, a repeated test in air resulting in fatigue life less than that of specimen 1 and similar to that of specimen 2 would not be considered unusual.

Although the mechanisms contributing to the reduced fatigue life underwater were not studied in detail, observation of the crack surfaces revealed that the specimen 2 showed more brittle behavior than specimen 1. Brittle behavior in specimen 2 was expected because, as discussed in Chapter 2, hydrogen embrittlement is a major factor in underwater fatigue. When comparing the crack surfaces at large crack lengths (during unstable growth), the indicators of ductile fracture were more pronounced for specimen 2. The crack surface for specimen 1 appeared more slanted and rougher than that of specimen 2.

4.3.2 Comparison of Specimens 2 and 3

Specimens 2 and 3 were compared to assess the effectiveness of the CFRP repair used underwater. Crack growth results for both specimens are presented together in Figure 4-39. The CFRP retrofit used underwater for specimen 3 provided a 31.1% increase in fatigue life over specimen 2, which was tested underwater with no repair. For small crack lengths before the crack reached the CFRP patch, the crack growth rate was noticeably lower for specimen 3 than specimen 2. This can be attributed to the increased cross-sectional stiffness and reduced nominal stress from the CFRP application. The influence of the crack closure effect that took place once the crack propagated beneath the CFRP is difficult to evaluate since crack length measurements could not be taken when the crack was growing beneath the patch. However, due to the substantial debonding of the CFRP patches on the north face of specimen 3, it is known that the crack closure effect was not fully utilized. It is believed that had the bond remained intact, a greater improvement in fatigue life would have been achieved.

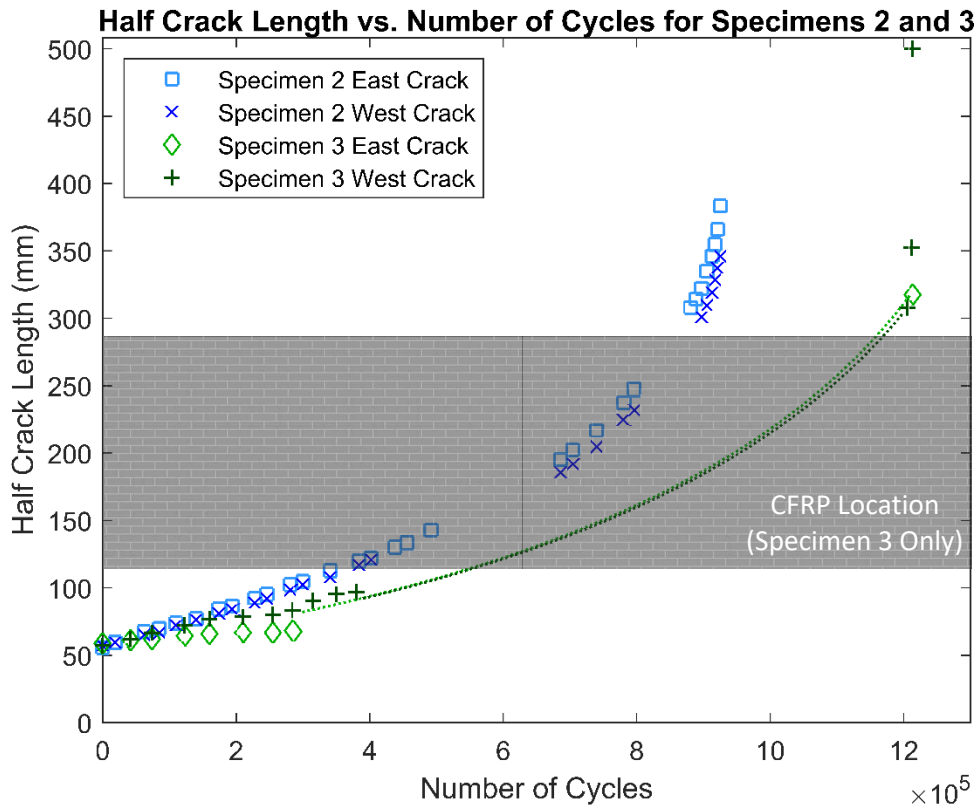


Figure 4-39. Comparison of crack growth for specimens 2 and 3

4.3.3 Comparison of Specimens 2 and 4

Specimens 2 and 4 were compared to assess the effectiveness of the BFRP repair used underwater. Crack growth results for specimen 2 and specimen 4 are presented together in Figure 4-40. The BFRP retrofit used underwater for specimen 4 provided a 90.9% increase in fatigue life over specimen 2 which was tested underwater with no repair. For small crack lengths before the crack reached the BFRP patch, the crack growth rate was noticeably lower for specimen 4 than specimen 2. This can be attributed to the increased cross-sectional stiffness and reduced nominal stress caused by the BFRP application. The BFRP further reduced the crack growth in comparison to specimen 2 by limiting the crack opening displacement once the crack propagated under the patch.

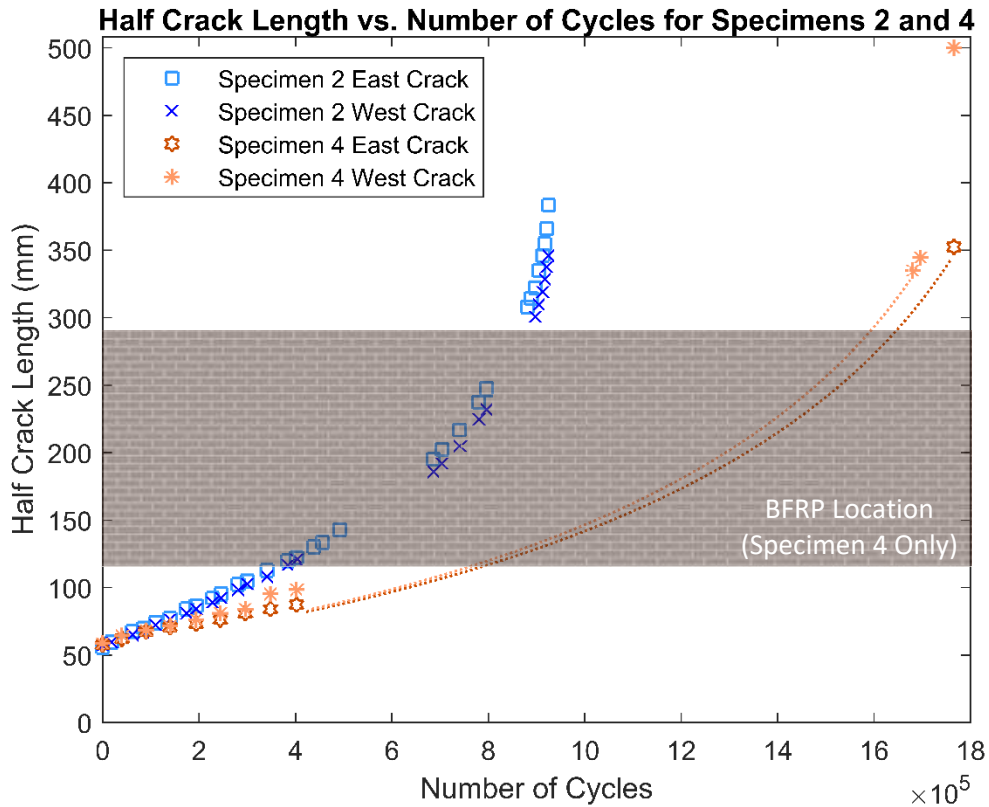


Figure 4-40. Comparison of crack growth for specimens 2 and 4

4.3.4 Comparison of Specimens 3 and 4

The use of CFRP and BFRP was compared by evaluating results from specimens 3 and 4. Results from specimen 3 and specimen 4 are shown together in Figure 4-41. At the early stage of the tests when the cracks had not yet reached the FRP patches, the crack growth rate was lower for specimen 3 due to the higher stiffness of the CFRP patches. As the crack continued to propagate, the BFRP did not experience debonding at the patch ends, and thus it was more effective at reducing the crack opening displacement than the CFRP, which debonded significantly.

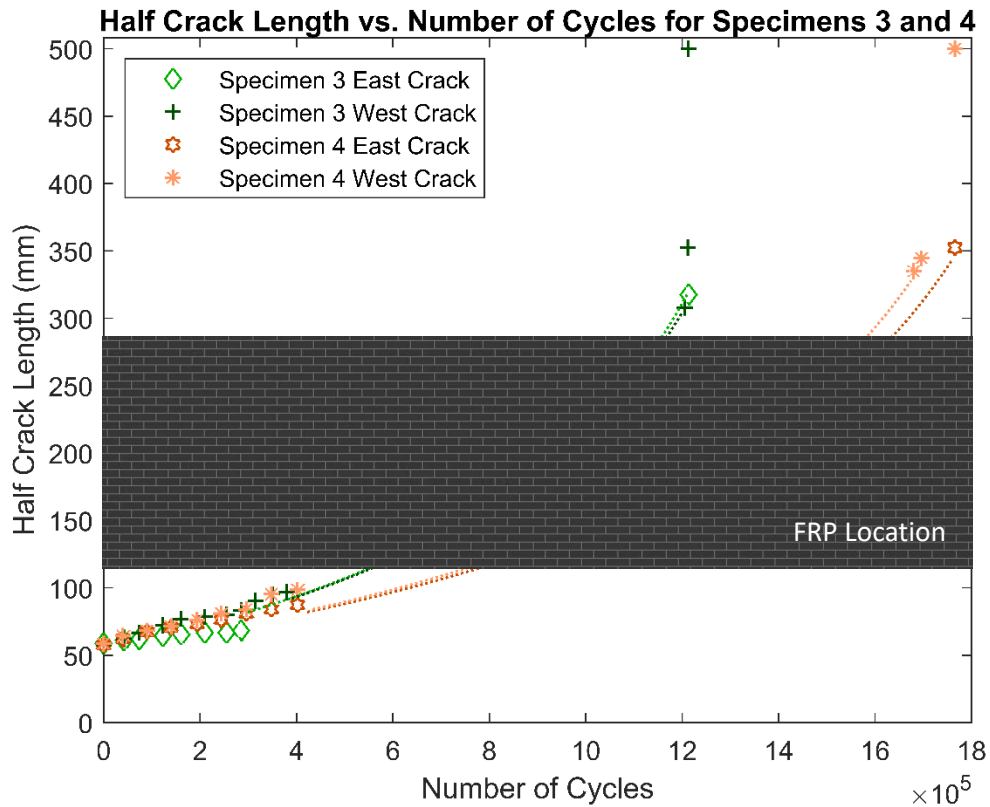


Figure 4-41. Comparison of crack growth for specimens 3 and 4

Had the CFRP used for specimen 3 not debonded, it likely would have limited the crack opening displacement better than the BFRP since the CFRP has higher stiffness. A single cause for the debonding of the CFRP cannot be clearly identified from the results of this study alone. Variations in the FRP application process, absence of any galvanic corrosion, or lower demand on the adhesive due to lower BFRP stiffness may have contributed to the better bond behavior observed when using BFRP.

Although not quantifiable, comparing the final failure methods of specimens 3 and 4 may provide some insight to the time dependence of adhesive deterioration underwater or debonding around the crack tip. On the south face of specimen 3, no debonding was detectable around the CFRP patch ends during the test, and fiber rupture occurred. For specimen 4, debonding at BFRP

patch ends was again not detectable, but bond failure occurred when the specimen fractured. Since the tensile strength of CFRP is higher than that of BFRP, either the bond strength or bond area for the patches on specimen 4 must have been lower than those for specimen 3, otherwise the BFRP in specimen 4 would have been expected to rupture. This indicates that the increased time needed for the specimen 4 crack to propagate beneath the patches may have caused the adhesive to deteriorate or the debonding around the crack tip may have been more substantial for specimen 4.

CHAPTER 5

CONCLUSION

5.1 Summary of Current Work

Four large-scale center-cracked tension specimens were fabricated for fatigue testing, and two of the for specimens were retrofitted using bonded FRP patches. CFRP, which has previously been used in various studies for fatigue crack repair in steel, was used to retrofit one specimen. Another specimen was retrofitted with BFRP, which has very limited previous use in civil engineering applications but does not react galvanically with steel as CFRP does. Special consideration was given to the quality of the bond between the steel and FRP because several previous studies indicate that FRP retrofits are limited by the bond. An underwater environment was introduced for the retrofitted specimens and one unretrofitted specimen to simulate the environment experienced by steel hydraulic structures and evaluate whether the retrofit methods are suitable for that environment.

Constant amplitude mode I fatigue tests were carried out for each specimen. Crack growth and FRP behavior were monitored throughout the tests. Results from the two unretrofitted specimens, only one of which was tested underwater, were compared to identify the reduction in fatigue life due to an underwater environment. The fatigue life of each retrofitted specimen was compared to that of the unretrofitted specimen tested underwater to determine the increase in life achieved by the retrofit. The use of BFRP as an alternative to CFRP was evaluated by comparing the two retrofitted specimens.

5.2 Conclusions

Results from the unrepaired specimens tested in air and water confirmed the expected outcome that crack growth is accelerated underwater. The decrease in fatigue life underwater of 10.3% was moderate when compared to some results reported in the literature and when considering the scatter in fatigue data. Although fatigue life was not reduced tremendously, the effect of the underwater environment on the steel needs to be considered for hydraulic structures since any decrease in life can become substantial throughout a long service life.

The retrofit methods using both CFRP and BFRP were shown to be viable for increasing fatigue life of a center-cracked panel with increases over the underwater unretrofitted specimen of 31.1% and 90.9%, respectively. BFRP performed better than CFRP due to the early debonding of the CFRP patches. Several factors, including the possibility of galvanic corrosion despite an insulating layer, increased demand on the adhesive due to higher modulus of CFRP, and variability in the application process, may have contributed to CFRP debonding. Both CFRP and BFRP may have experienced deterioration due to exposure to water. Effects of the underwater environment on the FRP materials cannot be directly identified from this study.

The higher stiffness of the CFRP was apparent when comparing crack growth with BFRP before the cracks reached the FRP patches. Had the bond remained intact for the CFRP, its higher stiffness most likely would have provided more fatigue life improvement than BFRP. Due to the very small sample size in this study and the variability in the application process, it cannot be concluded that CFRP would always debond in the conditions tested. For the same reasons, it cannot be concluded that BFRP will always perform better than CFRP. However, based on the positive results of the BFRP specimen, BFRP retrofit can be considered for future repair of fatigue damage in steel.

5.3 Recommendations for Future Work

Although the completed tests indicate that both CFRP and BFRP are viable repair options, the mechanisms caused by the underwater environment remain unclear. The extent to which saturation affected the adhesive properties and therefor contributed to the debonding in the specimen with CFRP is not known. Smaller scale testing to isolate the adhesive properties after water saturation is recommended. Exploring saturation over a longer time period is also recommended because time frame of the present tests was much shorter than the life span of a steel hydraulic structure. Since it is known that a threshold stress under which FRP will not debond exists, underwater bond fatigue tests for the FRP materials used would be useful for selecting future retrofit configurations. Additionally, the behavior of BFRP in both air and water is not well understood due to its limited prior use. Should BFRP be selected for further use, material properties, fatigue strength, and underwater durability should be tested on a small scale.

Based on the current results and the methods previously used by others, the following modifications for improving the retrofit method are recommended if additional large-scale tests of the same nature are performed:

- Modify the FRP patch geometry to cover the initial crack so that the crack closure mechanism can be better utilized and identify a method for detecting crack growth behind the FRP patch.
- Develop a mechanical clamping method to apply confining pressure to the FRP patch ends and reduce debonding
- Apply a sealant coating to the FRP patches to reduce exposure of the epoxies to water

Extending the large-scale testing method to account for multi-mode loading or more complex

geometry of the fatigue damaged component would also provide additional insight for future field use because many locations in SHS that experience fatigue damage are more complex than the configuration tested in the current work.

Since it is not feasible to conduct large-scale testing for all field application configurations, a method for predicting remaining fatigue life after a crack is repaired is desirable. Both numerical and analytical methods for predicting crack growth in air after applying FRP repairs exist, but for the purpose of rapidly assessing a needed repair, a quick analytical approach would more appropriate. An adaptation of the existing analytical models for growth of a repaired crack that accounts for the nominal stress reduction and crack closure effects of the FRP is suggested. Results from this thesis and any additional experimental work may be useful for making empirical modifications to account for underwater environmental factors.

REFERENCES

- Al Azzawi, M., Hopkins, P., Mullins, G., & Sen, R. (2018). FRP–Concrete Bond after 12-Year Exposure in Tidal Waters. *Journal of Composites for Construction*, 22(5), 04018031. [https://doi.org/10.1061/\(asce\)cc.1943-5614.0000864](https://doi.org/10.1061/(asce)cc.1943-5614.0000864)
- Bocciarelli, M., Colombi, P., Fava, G., & Poggi, C. (2009). Fatigue performance of tensile steel members strengthened with CFRP plates. *Composite Structures*, 87(4), 334–343. <https://doi.org/10.1016/j.compstruct.2008.02.004>
- BS 7910. (2015). BSI Standards Publication Guide to methods for assessing the acceptability of flaws in metallic structures. *BSI Standards Publication*, (UK), 490.
- Colombi, P. (2004). On the evaluation of compliance information for common crack growth specimens reinforced by composite patch. *International Journal of Fracture*. <https://doi.org/10.1023/B:FRAC.0000021043.74064.1a>
- Colombi, P., Bassetti, A., & Nussbaumer, A. (2003a). Analysis of cracked steel members reinforced by pre-stress composite patch. *Fatigue and Fracture of Engineering Materials and Structures*. <https://doi.org/10.1046/j.1460-2695.2003.00598.x>
- Colombi, P., Bassetti, A., & Nussbaumer, A. (2003b). Crack growth induced delamination on steel members reinforced by prestressed composite patch. *Fatigue and Fracture of Engineering Materials and Structures*, 26(5), 429–437. <https://doi.org/10.1046/j.1460-2695.2003.00642.x>
- Colombi, P., & Fava, G. (2015). Experimental study on the fatigue behaviour of cracked steel beams repaired with CFRP plates. *Engineering Fracture Mechanics*, 145, 128–142. <https://doi.org/10.1016/j.engfracmech.2015.04.009>
- Deng, J., & Lee, M. M. K. (2007). Fatigue performance of metallic beam strengthened with a

- bonded CFRP plate. *Composite Structures*, 78(2), 222–231.
<https://doi.org/10.1016/j.compstruct.2005.09.003>
- Dexter, R., Mahmoud, H., & Pilarski, P. (2005). Propagation of Long Cracks in Stiffened Box-sections under Bending and Stiffened Single Panels under Axial Tension. *International Journal of Steel Structures*, 5(3), 181–188.
- Dexter, R., Pilarski, P. J., & Mahmoud, H. N. (2003). Analysis of crack propagation in welded stiffened panels. *International Journal of Fatigue*, 25(9–11), 1169–1174.
<https://doi.org/10.1016/j.ijfatigue.2003.08.006>
- Dorigato, A., & Pegoretti, A. (2012). Fatigue resistance of basalt fibers-reinforced laminates. *Journal of Composite Materials*, 46(15), 1773–1785.
<https://doi.org/10.1177/0021998311425620>
- Gangel, R. E. (2011). *Use Of CFRP Overlays to Repair Fatigue Damage in Steel Bridge Girders and Components*. University of Kansas.
- Gangloff, R. (2009). Environmental Cracking-Corrosion Fatigue. In *Corrosion Tests and Standards: Application and Interpretation—Second Edition*.
<https://doi.org/10.1520/mnl11032m>
- Hollaway, L. C., & Cadei, J. (2002). Progress in the technique of upgrading metallic structures with advanced polymer composites. *Progress in Structural Engineering and Materials*, 4(2), 131–148. <https://doi.org/10.1002/pse.112>
- Jayasuriya, S., Bastani, A., Kenno, S., Bolisetti, T., & Das, S. (2018). Rehabilitation of Corroded Steel Beams Using BFRP Fabric. *Structures*, 15(March), 152–161.
<https://doi.org/10.1016/j.istruc.2018.06.006>
- Jones, S. C., & Civjan, S. A. (2003). Application of Fiber Reinforced Polymer Overlays to Extend

- Steel Fatigue Life. *Journal of Composites for Construction*, 7(4), 331–338.
[https://doi.org/10.1061/\(asce\)1090-0268\(2003\)7:4\(331\)](https://doi.org/10.1061/(asce)1090-0268(2003)7:4(331))
- Kang, D. H., Lee, J. K., & Kim, T. W. (2011). Corrosion fatigue crack propagation of high-strength steel HSB800 in a seawater environment. *Procedia Engineering*, 10, 1170–1175.
<https://doi.org/10.1016/j.proeng.2011.04.195>
- Liu, F. T., He, G. H., & Xiong, J. H. (2017). Experimental study on durability of FRP sheets under wet-dry cycles in various solutions. *Procedia Engineering*, 210, 61–70.
<https://doi.org/10.1016/j.proeng.2017.11.049>
- Liu, H., Al-Mahaidi, R., & Zhao, X.-L. (2009). Experimental study of fatigue crack growth behaviour in adhesively reinforced steel structures. *Composite Structures*, 90, 12–20.
<https://doi.org/10.1016/j.compstruct.2009.02.016>
- Liu, H., Xiao, Z., Zhao, X.-L., & Al-Mahaidi, R. (2009). Prediction of fatigue life for CFRP-strengthened steel plates. *Thin-Walled Structures*. <https://doi.org/10.1016/j.tws.2008.10.011>
- Liu, H., Zhao, X., Almahaidi, R., & Rizkalla, S. (2007). Analytical bond models between steel and normal modulus CFRP. *Fourth International Conference on Advances in Steel Structures, II*, 1545–1552. <https://doi.org/10.1016/b978-008044637-0/50230-4>
- Liu, H., Zhao, X. L., & Al-Mahaidi, R. (2005). The effect of fatigue loading on bond strength of CFRP bonded steel plate joints. *The International Symposium on Bond Behaviour of FRP in Structures*, (March 2015), 451–456.
- Long, M., Djelal, C., Kesteloot, S., Bigourdan, B., Gac, P. Y. Le, & Szulc, J. (2012). Durability of Cfrp-Concrete Bonding in a Marine Environment, (June), 24–28.
- Lozano, C. M., & Riveros, G. A. (2019). Effects of adhesive bond-slip behavior on the capacity of innovative FRP retrofits for fatigue and fracture repair of hydraulic steel structures.

- Materials*, 12(9). <https://doi.org/10.3390/ma12091495>
- Mahmoud, H., Chulahwat, A., & Riveros, G. (2018). Fatigue and fracture life-cycle cost assessment of a Miter gate with multiple cracks. *Engineering Failure Analysis*, 83(September 2017), 57–74. <https://doi.org/10.1016/j.engfailanal.2017.09.008>
- Mahmoud, H. N., Como, A., & Riveros, G. A. (2014). Fatigue Assessment of Underwater CFRP-Repaired Steel Panels using Finite Element Analysis, (September).
- Mahmoud, H. N., & Dexter, R. (2005). Propagation rate of large cracks in stiffened panels under tension loading. *Marine Structures*, 18(3), 265–288. <https://doi.org/10.1016/j.marstruc.2005.09.001>
- Mahmoud, H. N., & Riveros, G. A. (2013). *Fatigue Repair of Steel Hydraulic Structures (SHS) using Carbon Fiber Reinforced Polymers (CFRP): Feasibility Study*.
- Mahmoud, H. N., Riveros, G. A., Memari, M., Valsangkar, A., & Ahmadi, B. (2018). Underwater Large-Scale Experimental Fatigue Assessment of CFRP-Retrofitted Steel Panels. *Journal of Structural Engineering (United States)*, 144(10), 1–12. [https://doi.org/10.1061/\(ASCE\)ST.1943-541X.0002184](https://doi.org/10.1061/(ASCE)ST.1943-541X.0002184)
- Mahmoud, H., & Riveros, G. (2014). Fatigue reliability of a single stiffened ship hull panel. *Engineering Structures*, 66, 89–99. <https://doi.org/10.1016/j.engstruct.2014.02.007>
- Matta, F., Karbhari, V. M., & Vitaliani, R. (2005). Tensile response of steel/CFRP adhesive bonds for the rehabilitation of civil structures. *Structural Engineering and Mechanics*, 20(5), 589–608. <https://doi.org/10.12989/sem.2005.20.5.589>
- Mertz, D. R., & Gillespie, J. W. (2002). *Rehabilitation of steel bridge girders using advanced composite materials. NCHRP-IDEA Program Project Final Report*. Retrieved from <https://trid.trb.org/view.aspx?id=481482>

- Misawa, T., & Kobayashi, Y. (2017). Effect of pH on Corrosion Fatigue Crack Propagation in a Low Carbon Steel. *Corrosion Engineering*. https://doi.org/10.3323/jcorr1974.25.8_493
- Monfared, A., Soudki, K., & Walbridge, S. (2008). CFRP reinforcing to extend the fatigue lives of steel structures. *Fourth International Conference on FRP Composites in Civil Engineering (CICE2008), Zurich, Switzerland, 22–24*. Retrieved from http://www.iifc-hq.org/proceedings/CICE_2008/papers/5.D.2.pdf
- Morgantini, M., Okorokov, V., Gorash, Y., Mackenzie, D., & Van Rijswick, R. (2018). The Effect of Fresh Water Solution on Fatigue Strength of Low Carbon Steel (pp. 22–26).
- Nozaka, K., Shield, C. K., & Hajjar, J. F. (2005). Effective Bond Length of Carbon-Fiber-Reinforced Polymer Strips Bonded to Fatigued Steel Bridge I-Girders. *Journal of Bridge Engineering, 10*(2), 195–205. [https://doi.org/10.1061/\(asce\)1084-0702\(2005\)10:2\(195\)](https://doi.org/10.1061/(asce)1084-0702(2005)10:2(195))
- Riveros, G. A., Mahmoud, H., Memari, M., Lozano, C., Valsangkar, A., & Ahmadi, B. (2019). *Underwater Fatigue Repair of Steel Panels Using Carbon Fiber Reinforced Polymers*. <https://doi.org/10.13140/RG.2.2.21236.30081>
- Riveros, G. A., Mahmoud, H. N., & Lozano, C. M. (2018). Fatigue repair of underwater navigation steel structures using Carbon Fiber Reinforced Polymer (CFRP). *Engineering Structures, 173*(July), 718–728. <https://doi.org/10.1016/j.engstruct.2018.07.016>
- Salivar, G. C., Creighton, D. L., & Hoepfner, D. W. (1981). Effect of Frequency and Environment on Fatigue-Crack Propagation of SA533B-1 Steel. *Engineering Fracture Mechanics, 14*, 337–352.
- Shield, C., Nozaka, K., & Hajjar, J. (2004). *Repair of Fatigued Steel Bridge Girders with Carbon Fiber Strips*.
- Tavakkolizadeh, M., & Saadatmanesh, H. (2001). Galvanic Corrosion of Carbon and Steel.

- Journal of Composites for Construction*, 5(August), 200–210.
- Tavakkolizadeh, M., & Saadatmanesh, H. (2003). Fatigue Strength of Steel Girders Strengthened with Carbon Fiber Reinforced Polymer Patch. *Journal of Structural Engineering*, 129(2), 186–196. [https://doi.org/10.1061/\(asce\)0733-9445\(2003\)129:2\(186\)](https://doi.org/10.1061/(asce)0733-9445(2003)129:2(186))
- U.S. Army Corps of Engineers (USACE). (2010). *Advanced Reliability analysis of fatigue cracking in horizontal frame miter gates*. <https://doi.org/10.15713/ins.mmj.3>
- Vatandoost, F. (2010). Fatigue Behaviour of Steel Girders Strengthened with Prestressed CFRP Strips, (March).
- Wu, C., Zhao, X., Al-mahaidi, R., Emdad, M. R., & Duan, W. (2012). Fatigue Tests of Cracked Steel Plates Strengthened with UHM CFRP Plates, 15(10), 1801–1815. <https://doi.org/10.1260/1369-4332.15.10.1801>
- Wu, C., Zhao, X. L., Al-Mahaidi, R., & Duan, W. H. (2013). Effects of CFRP bond locations on the Mode I stress intensity factor of centre-cracked tensile steel plates. *Fatigue and Fracture of Engineering Materials and Structures*. <https://doi.org/10.1111/j.1460-2695.2012.01708.x>
- Wu, G., Wang, H.-T., Wu, Z.-S., Liu, H.-Y., & Ren, Y. (2012). Experimental Study on the Fatigue Behavior of Steel Beams Strengthened with Different Fiber-Reinforced Composite Plates. *Journal of Composites for Construction*, 16(2), 127–137. [https://doi.org/10.1061/\(ASCE\)CC.1943-5614](https://doi.org/10.1061/(ASCE)CC.1943-5614)
- Wu, Z., Wang, X., Iwashita, K., Sasaki, T., & Hamaguchi, Y. (2010). Tensile fatigue behaviour of FRP and hybrid FRP sheets. *Composites Part B: Engineering*, 41(5), 396–402. <https://doi.org/10.1016/j.compositesb.2010.02.001>
- Zhao, X. L., & Zhang, L. (2007). State-of-the-art review on FRP strengthened steel structures. *Engineering Structures*, 29(8), 1808–1823. <https://doi.org/10.1016/j.engstruct.2006.10.006>

Zheng, Y., Ye, L., & Lu, X. (2006). Experimental Study on Fatigue Behavior of Tensile Steel Plates Strengthened with CFRP Plates. *Third International Conference on FRP Composites in Civil Engineering*, (Cice), 5.